CML 81-1 NASA CR-165460

INDENTATION LAW FOR COMPOSITE LAMINATES

by

S.H. Yang and C.T. Sun

July 31, 1981

COMPOSITE MATERIALS LABORATORY

PURDUE UNIVERSITY
School of Aeronautics and Astronautics
West Lafayette, Indiana 47907

CML 81-1 NASA CR-165460

INDENTATION LAW FOR COMPOSITE LAMINATES

by

S.H. Yang and C.T. Sun

July 31, 1981

NASA GRANT NSG 3185

1. Report No.	2. Government Accession No.	3. Recipient's Catalog No.
CR 165460		

4. Title and Subtitle	5. Report Date
Indentation Law for Composite Laminates	July 31, 1981
	6. Performing Organization Code

7. Author(s)	8. Performing Organization Report No.
S. H. Yang and C. T. Sun	
	10. Work Unit No.

9. Performing Organization Name and Address	11. Contract or Grant No.
Purdue University School of Aeronautics and Astronautics West Lafayette, IN 47907	NSG3185
	13. Type of Report and Period Covered
12. Sponsoring Agency Name and Address	Topical Report
National Aeronautics & Space Administration Washington DC 20546	14. Sponsoring Agency Code

15. Supplementary Notes Project Manager: C. C. Chamis
Structures and Mechanical Technologies Division, Mail Stop 49-6
NASA Lewis Research Center
21000 Brookpark Road
Cleveland, OH 44135

16. Abstract

Static indentation tests are described for glass/epoxy and graphite/epoxy composite laminates with steel balls as the indentor. Beam specimens clamped at various spans were used for the tests. Loading, unloading, and reloading data were obtained and fitted into power laws. Results show that (1) contact behavior is not appreciably affected by the span; (2) loading and reloading curves seem to follow the 1.5 power law; and (3) unloading curves are described quite well by a 2.5 power law. In addition values were determined for the critical indentation, α_{cr}, which can be used to predict permanent indentations in unloading. Since α_{cr} only depends on composite material properties, only the loading and an unloading curve are needed to establish the complete loading-unloading-reloading behavior.

17. Key Words (Suggested by Author(s))	18. Distribution Statement
Composite laminates, indentation test, contact law, loading, unloading, reloading	Unclassified, Unlimited

19. Security Classif. (of this report)	20. Security Classif. (of this page)	21. No. of Pages	22. Price*
Unclassified	Unclassified		

* For sale by the National Technical Information Service, Springfield, Virginia 22161

TABLE OF CONTENTS

LIST OF TABLES

LIST OF FIGURES

NOMENCLATURE

D_S	Diameter of the spherical indentor
E_1	Longitudinal modulus of elasticity
E_2	Transverse modulus of elasticity
E_S	Young's modulus for sphere
E_t	Young's modulus for target
F	Contact force
F_m	Maximum contact force at unloading
G_{12}	In-plane shear modulus of elasticity
R_S	Radius of sphere
k	Contact coefficient
k_1	Reloading coefficient
k'	Contact coefficient with the unit of stress
s	Unloading coefficient
α	Indentation
α_o	Permanent indentation
α_{cr}	Critical indentation
α_m	Maximum identation at unloading
ν_S	Poisson's ratio of sphere
ν_t	Poisson's ratio of target

1. Introduction

It is well recognized that composite laminates are susceptible to damage resulting from impact of foreign objects. In general, hard and soft objects result in different failure modes. If the object is relatively rigid and small, then the contact time is short and extensive damage occurs in the neighborhood of the contact region. The extent of damage obviously depends on the contact force between the object and the target composite. An accurate account of the contact force and indentation is necessary to quantify the impact damage.

Direct measurement of the dynamic contact force is not an easy task due to the wide range of impact velocities and other parameters, and limitations of experimental techniques. The objective of this study is to determine experimentally static indentation laws for epoxy-based composite laminates in contact with steel balls and then model them in power laws.

The most famous elastic contact law, $F = k\alpha^{3/2}$, was derived by Hertz [1] for the contact of two spheres of elastic isotropic materials based upon theory of elasticity. The contact between a sphere and a half-space is a limiting case. Since this contact law is derived based upon the contact of elastic spheres, one faces several uncertainties when applying it to laminated composites. First, most laminated composites in use can not be adequately represented by a half-space. Second, the anisotropic and nonhomogeneous property of laminated composites may alter the form of the law. Third, the strain rate which is not accounted for by the Hertzian law may have significant effects on the $F - \alpha$ relation.

Except for the strain rate effect, the first two uncertainties may be

cleared by analyzing the exact contact problem of a sphere pressed into a laminated composite by using three-dimensional elasticity. However, experience tells us that analytical solutions for such contact problems are extremely difficult to obtain especially if permanent deformations are to be accounted for during unloading. Since unloading paths are important as far as the local damage zone is concerned, in this study, an experimental approach is taken to determine the law of contact for composites. However, the strain rate effect is neglected.

2. Hertzian Law of Contact

When two solid bodies are in contact, deformation takes place in the contact zone and the contact force results. Once the contact force is obtained, conventional methods for stress analysis can be used to find the stress distribution in the bodies. Determination of the contact force-indentation relationship often becomes the most important step in analyzing the contact problem.

A special case of the Hertz contact problem is the contact of an elastic sphere and an elastic half space. The contact force F and the indentation depth α have the relation

$$F = k\,\alpha^{3/2} \tag{1}$$

where

$$k = (4/3)\,(R_s)^{1/2}\,[(1-\nu_s^{\,2})/E_s + (1-\nu_t^{\,2})/E_t\,]^{-1} \tag{2}$$

In equation (2), R_s is the radius of the sphere, ν is the Poisson's ratio, E is the Young's modulus, and subscripts s and t indicate the sphere and the target, respectively. Equation (1) is usually called the Hertzian law of contact for a sphere in contact with a half-space.

The 1.5 power given by equation (1) was found to be valid by Willis [2] for a rigid sphere pressed on a transversely isotropic half-space. A modified contact law with

$$k = (4/3)\ (R_s)^{1/2}\ \ [(1-\nu_s^{\,2})/E_s + 1/E_2]^{-1} \qquad (3)$$

was employed by Sun [3] for a study on impact of laminated composites. In equation (3), R_s, ν_s and E_s are the radius, the Poisson's ratio and the Young's modulus of the isotropic sphere, respectively, and E_2 is the modulus of elasticity transverse to the fiber-direction in the fiber-reinforced composite.

A more general form for the contact law was proposed by Meyer [4] as

$$F = k\ \alpha^n \qquad (4)$$

which has been found suitable for many static indentations. It is obvious that when n = 1.5 and k given by equation (2) this relation reduces to the Hertzian law for isotropic bodies.

Permanent indentation in composite targets often takes place even at relatively low loading levels. Thus, the aforementioned indentation laws for elastic bodies are valid only for the loading process. To account for the permanent deformation, the following power law was suggested by Crook [5].

$$F = F_m[(\alpha - \alpha_o)/(\alpha_m - \alpha_o)]^q \qquad (5)$$

where F_m is the maximum contact force just before unloading, α_m is the indentation corresponding to F_m, and α_o is the permanent indentation during this loading-unloading cycle. This unloading law was used by Barnhart and Goldsmith [6] for impact of a steel ball onto an armor plate.

3. Experimental Procedures

The experimental set-up is shown schematically in Fig. 1. The indentation was measured by a dial gage that permits reading up to 1/5000 in. The dial gage was mounted on a 'C' bracket fixed to the loading piston so that only the relative displacement between the indentor and the beam was recorded. The load applied pneumatically was measured using a load cell and a strain indicator. Two steel balls of diameters 6.35 mm (0.25") and 12.7 mm (0.5") were used as indentors. In all tests the beam was clamped at both ends.

Two types of laminated composites have been tested, namely glass/epoxy and graphite/epoxy. The glass/epoxy was Scotch Ply 1002 by the 3M Company. It contained 10 0°-plies and 9 90°-plies which alternate in the layup with one 0°-ply on top and on at the bottom. The thickness of the beam was 4.83 mm (0.19") and the width 38.1 mm (1.5"). The graphite/epoxy specimens were $[0/45/0/-45/0]_{2s}$ laminates. The thickness was 2.54 mm (0.1 in.). Two specimen widths were considered, namely 25.4 mm (1.0 in.) and 38.1 mm (1.5 in.). Their material properties are given as follows:

Glass/Epoxy:

$$E_1 = 39.3\text{GPa } (5.7 \times 10^6 \text{ psi})$$
$$E_2 = 8.27\text{GPa } (1.2 \times 10^6 \text{ psi})$$
$$G_{12} = 4.14\text{GPa } (0.6 \times 10^6 \text{ psi}) \qquad (6)$$
$$\nu_{12} = 0.26$$

Graphite/Epoxy:

$$E_1 = 120.7\text{GPa } (17.5 \times 10^6 \text{ psi})$$
$$E_2 = 7.93\text{GPa } (1.15 \times 10^6 \text{ psi})$$
$$G_{12} = 5.52\text{GPa } (0.80 \times 10^6 \text{ psi}) \qquad (7)$$
$$\nu_{12} = 0.30$$

where subscripts 1 and 2 indicate directions parallel and perpendicular to the fiber, respectively.

Data were recorded in steps of about 2 to 5 units in the dial gage. Readings on the dial gage and strain indicator were taken about 10 to 20 seconds after the load was increased by one step.

4 Experimental Results and Modeling

4.1 Loading Curve

(A) Glass/Epoxy

For the glass/epoxy laminate, three sets of loading data were obtained for each span with a 6.35mm (0.25") diameter indentor. These data were used to determine the best fit for the power law, equation (4), using the least square method. A typical set of the data is presented in Fig. 2. The power indexes

for all three cases appear to be rather close to that of the classical Hertzian law for isotropic solids, i.e., n = 1.5. For this reason, we set n = 1.5, and then determined the contact coefficient k by using the least square fit. One of the resulting curves is shown in Fig. 3. The curves seem to fit the data very well also.

Table 1 summarizes the indentation law (the loading portion) obtained from the experimental data for the glass/epoxy laminate. It is interesting to note that with n = 1.5, the values of k for different spans are almost a constant. This may be taken as an indication that the indentation law is independent of span. In other words, the bending stress in the range of these experiments does not influence the contact rigidity.

In Table 1, the modified Hertzian law, equation (3), is also presented using the material constants given in equation (6). It is found that the value of k is higher than the experimental values. However, it does provide a good estimate of the contact behavior.

(B) Graphite/Epoxy

For the 6.35 mm (0.25") diameter indentor, three sets of data were obtained for each span, while for the 12.7 mm (0.5") diameter indentor, except for one case, two sets of data were collected. The value of n was set equal to 1.5. The values of k fitted using each set of unloading data and all three (or two) sets of data are presented in Table 2. The corresponding modified Hertzian law are also shown in Table 2 for comparison. In Figs. 4-7 four typical sets of the experimental data are compared with the loading curves predicted by the power law.

From the values of k for the two indentors, it was found that k for 12.7 mm (0.5") indentor is about 1.8 times larger than that for the 6.35 mm (0.25") indentor. According to the Hertzian law, k is proportional to the square root of the diameter of the indentor and the increase in the k value should be 1.414.

From the experimental results, it is difficult to assess the effect of the specimen width. However, the variation in k for the 12.7 mm (0.5") indentor with respect to span and width seem to be smaller than that for the 6.37 mm (0.25") indentor.

4.2 Unloading Curve

(A) Glass/Epoxy

From the test results we observed that permanent deformation occurred after an indentation test at very low load levels. The unloading paths were very different from the loading path as can be seen from Fig. 8. The unloading curves were modeled by using equation (5) in which q and α_o were determined from experimental data. Since the permanent indentation α_o was difficult to measure, the whole set of data for each unloading was taken to determine q and α_o by the least square method. The results showed that the values of q thus obtained varied between 2.0 and 3.0. It was found that q increased as the loading level increased. For q = 3.0 and q = 2.5, equation (5) seems to fit the overall data quite well as shown by Figs. 8-9. However, if q = 3.0, the value of α_o might become negative in some cases. For this reason, q = 2.5 was chosen.

It should be pointed out that the value of α_o obtained in this manner may not be the true permanent indentation. It is a value which can make

the power law given by equation (5) fit the total data in an unloading path.

Since α_o depends on where the unloading begins, it seems that many unloading tests have to be performed in order that the unloading law given by equation (5) can be useful. In other words, the relation between α_o and F_m must be established.

Setting q = 2.5, we rewrite equation (5) in the following form

$$F = s\ (\alpha - \alpha_o)^{5/2} \tag{8}$$

where

$$s = F_m/(\alpha_m - \alpha_o)^{5/2} \tag{9}$$

is an unloading rigidity. A fitting of the data can be obtained by fixing the value of s in all the unloading paths for finding α_o. In doing so, we imply that the unloading rigidity s remains unchanged. Such assumption will greatly simplify the modeling of unloading. With this in mind, it is assumed that

$$k/s = \alpha_{cr} \tag{10}$$

is a constant for a given material system and size of the indentor.

From the loading curve we have

$$F_m = k\ \alpha_m^{3/2} \tag{11}$$

By combining equations (9) through (11) the following equation is obtained

$$\alpha_o/\alpha_m = 1 - (\alpha_{cr}/\alpha_m)^{2/5} \tag{12}$$

This equation can be used to calculate α_o as a function of α_m.

From equation (12) it is easy to see that

$$\alpha_o \geq 0 \quad \text{as} \quad \alpha_m \geq \alpha_{cr} \tag{13}$$

i.e., when indentation passes the value α_{cr} then permanent deformation occurs. To avoid results which are not physically meaningful, we set

$$\alpha_o = 0 \quad \text{if} \quad \alpha_m \leq \alpha_{cr}$$

Hence, according to this model, α_{cr} can be regarded as the 'yield' point in indentation.

Since the energy dissipation in each loading-unloading cycle is of the main interest in this study, it is sensible to select α_o in the unloading law so that the area under the unloading curve is equal to that calculated from the experimental data. One set of the unloading curves predicted by using the unloading law with this "area fit" is presented in Fig. 10. If these values of α_o are substituted into equation (9), a range of value for s is obtained. By using the averaged value for s, the value for α_{cr} is obtained from equation (10) as following

$$\alpha_{cr} = 10.16 \times 10^{-2} \text{mm} \ (4.0 \times 10^{-3} \text{ inch}) \tag{14}$$

The corresponding α_o can then be obtained from equation (12). The unloading curves corresponding to those shown in Fig. 10 using this α_{cr} are shown in Fig. 11. These curves seem to yield good agreement with experimental data. It was noted that a small variation in α_{cr} would not have any appreciable effect on the unloading curve.

Table 3 summarizes the comparison of the areas under the unloading curves predicted by the direct area fit and the use of α_{cr}. The values of α_o obtained from the two approaches are also listed for comparison. The approach using α_{cr} is found to be adequate in estimating the area under the unloading curve.

(B) Graphite/Epoxy

For the graphite/epoxy laminate, again q = 2.5 was used for the unloading law. Figs. 12-13 show some of the experimental data and the predicted unloading curves using values of α_o obtained by matching the area under the unloading curve.

The best value of α_{cr} for graphite/epoxy was found to be

$$\alpha_{cr} = 8.03 \times 10^{-2} \text{ mm } (3.16 \times 10^{-3} \text{ inch}) \qquad (15)$$

for both sizes of indentor. The unloading curves predicted by using this α_{cr} value corresponding to the cases presented in Figs. 12-13 are presented in Figs. 14-15. Excellent agreement with experimental results was noted. The results for the 6.25 mm(0.25") and 12.7 mm(0.5") indentors obtained according to the above two approaches are summarized in Table 4 and Table 5, respectively. Note that the loading curves in Figs. 12-15 were plotted using a particular set of loading data for each case rather than the average value.

The fact that α_{cr} is not dependent on the indentor size is interesting. This may imply that α_{cr} is a material property similar to the yield stress for mild steel.

4.3 Reloading Curve

In the case where multiple impacts occur, the reloading behavior must be modeled. The reloading experiment was performed only on the graphite/epoxy laminate with the 1.27 cm (0.5") diameter indentor.

The reloading law was assumed to be in the form

$$F = k_1 (\alpha - \alpha_o)^p \tag{16}$$

where k_1 is a reloading rigidity. From the experimental data, $p = 1.5$ seemed to have fitted the data best.

It was observed that when the loading level was not too high, then the reloading curve always returned to where the unloading began. If such condition is imposed on the reloading law given by equation (16), then we have

$$k_1 = F_m/(\alpha_m - \alpha_o)^{3/2} \tag{17}$$

Thus the reloading rigidity k_1 is determined if the unloading condition (F_m, α_m, and α_o) is specified. In other words, there is no need to perform reloading experiments to find the reloading rigidity k_1.

Figs. 16-17 show typical experimental data and the predicted reloading curves obtained according to equations (16-17). Good agreement is noted.

Table 6 shows a number of values of k_1 computed according to equation (17). It is seen that these values are quite close to the loading rigidity k for small α_o. However, for higher loading levels, a substantial deviation exists between these two values.

5 Discussion

From the results for the graphite/epoxy laminate, some scatter in the value of k in the loading law is noted even when the same material properties, indentor, and loading condition are used. This could be attributed to local material nonhomogeneity in the composite.

Being accustomed to the use of stress-strain relation to describe solid material properties one would attempt to modify the loading law into a similar form. A natural step that one would take is to divide the contact force F by a reference area and the indentation α by a reference length. Using the projection of the contact area, $2\pi D_s \alpha$, as the reference area and the critical indentation α_{cr} as the reference length, we obtain from the indentation law the following

$$F/(\pi D_s \alpha) = [k\ \alpha_{cr}^{1/2}/(\pi D_s)](\alpha/\alpha_{cr})^{1/2} \tag{18}$$

Such form does not offer any advantage over the original form.

If the reference area $\pi D_s \alpha_{cr}$, the projection of the contact area when $\alpha = \alpha_{cr}$, is used instead, then the indentation law can be modified into

$$F' = k'\ (\alpha')^{3/2} \tag{19}$$

where

$$F' = F/(D_s \alpha_{cr}) \tag{20}$$

$$k' = k\ \alpha_{cr}^{1/2}/D_s \tag{21}$$

$$\alpha' = \alpha/\alpha_{cr} \tag{22}$$

Note that F' has the unit of stress. Values of k' for the graphite/epoxy laminate are summarized in Table 7.

From equation (21), it is evident that k' becomes a constant if k is proportional to the diameter of the indentor. From our experimental data for the two indentor sizes, it appears that k is proportional to $(D_s)^{0.85}$ as opposed to $(D_s)^{0.5}$ predicted by the classical Hertzian law. More experimental data from more indentor sizes are needed to establish the relationship between k and the size of indentor.

In summary, we have established loading, unloading and reloading laws for glass/epoxy and graphite/epoxy laminates in contact with steel balls. For loading and reloading, 1.5 power laws seem to fit the data and for unloading, 2.5 power seems adequate. By using the critical indentation, α_{cr}, permanent indentations α_o can be related to the unloading force F_m, and consequently only one unloading curve has to be established experimentally. Further, since α_{cr} seems to depend only on the material properties, only one unloading test needs to be conducted for each material system. For reloading, if equation (16) is employed, no unloading tests are needed to establish the unloading law.

6. References

[1] Timoshenko, S., Theory of Elasticity, McGraw-Hill, New York, 3rd edition, 1970, pp. 409-420.

[2] Willis, J.R., "Hertzian Contact of Anisotropic Bodies," Journal of Mechanics and Physics of Solids, Vol. 14, 1966, pp. 163-176.

[3] Sun, C.T., "An Analytical Method for Evaluation of Impact Damage Energy of Laminated Composites," in Composite Materials: Testing and Design (Fourth Conference), ASTM, STP 617, American Society for Testing and Materials, 1977, pp. 427-440.

[4] Goldsmith, W., Impact, Edward Arnold, London, 1960, pp. 82-89.

[5] Crook, A.W., "A Study of Some Impacts Between Metal Bodies by a Piezoelectric Method," Proceedings of Royal Society, London, A 212, 1952, p.377.

[6] Barnhart, K.E., and Goldsmith, W., "Stresses in Beams during Transverse Impact," Journal of Applied Mechanics, Vol. 24, 1957, pp. 440-446.

Acknowledgments

This work was sponsored by NASA-Lewis Research Center under Grant No. NSG3185 with Purdue University. The authors are grateful to Dr. C.C. Chamis of NASA-Lewis Research Center for his valuable suggestions during the course of this research.

Table 1-Loading law $F=k\alpha^n$ for glass/epoxy with 6.35 mm diameter indentor, F in N and α in mm (F in lb and α in inch).

Glass/Epoxy:$[(0/90)_4/0/90/0/(90/0)_4]$				
Span, mm (in.)		50.8 (2.0)	101.6 (4.0)	152.4(6.0)
Least Squares Fit	n	1.54	1.54	1.66
	k, N/mm^n ($lb./in^n$)	1.70×10^4 (5.57×10^5)	1.71×10^4 (5.60×10^5)	2.00×10^4 (6.55×10^5)
1.5 Power Fit	n	1.5	1.5	1.5
	k, $N/mm^{1.5}$ ($lb/in.^{1.5}$)	1.60×10^4 (4.62×10^5)	1.61×10^4 (4.63×10^5)	1.60×10^4 (4.59×10^5)
Modified Hertzian Law, Eq. (3)	$F = 1.90 \times 10^4 \alpha^{1.5}$, F in N, α in mm ($F = 5.46 \times 10^5 \alpha^{1.5}$, F in lb, α in inch) E_s = 207 GPa (30×10^6 psi), ν_s = 0.3 E_2 = 8.27 GPa (1.2×10^6 psi), R_s=3.175mm(0.125 in)			

Table 2-Loading law $F=k\alpha^{1.5}$ for $[0/45/0/-45/0]_{2s}$ graphite/epoxy; F in N and α in mm (F in lb and α in inch).

Ball Dia., mm (in.)	6.35 (0.25)				12.7 (0.50)			
Span, mm (in.)	50.8 (2.0)		101.6 (4.0)		50.8 (2.0)		101.6 (4.0)	
Width, mm (in.)	25.4(1.0)	38.1(1.5)	25.4(1.0)	38.1(1.5)	25.4(1.0)	38.1(1.5)	25.4(1.0)	38.1(1.5)
k, 10^4 N/mm$^{1.5}$ (10^5 lb/in.$^{1.5}$)	2.00 (5.77)	1.82 (5.23)	1.78 (5.14)	2.14 (6.17)	3.30 (9.51)	3.36 (9.67)	3.33 (9.59)	3.68 (10.59)
	2.13 (6.13)	1.83 (5.27)	1.82 (5.23)	2.20 (6.34)	3.59 (10.33)	3.31 (9.53)	3.18 (9.15)	3.48 (10.01)
	2.06 (5.92)	1.85 (5.33)	1.83 (5.28)	2.32 (6.68)	3.56 (10.24)			
k, Group Fit 10^4 N/mm$^{1.5}$ (10^5 lb/in.$^{1.5}$)	2.06 (5.94)	1.85 (5.33)	1.81 (5.22)	2.19 (6.29)	3.47 (9.98)	3.34 (9.62)	3.23 (9.30)	3.60 (10.37)
Modified Hertzian Law, Eq.(3)	$F = 1.82 \times 10^4 \alpha^{1.5}$ ($F = 5.24 \times 10^5 \alpha^{1.5}$)				$F = 2.57 \times 10^4 \alpha^{1.5}$ ($F = 7.41 \times 10^5 \alpha^{1.5}$)			
	E_s = 207 GPa (30 x 10^6 psi), ν_s = 0.3, E_2 = 7.93 GPa (1.15 x 10^6 psi)							

Table 3-Values of α_0 and area under the unloading curve by different fits for glass/epoxy

Span, mm (in.)		50.8 (2.0)				101.6 (4.0)				152.4 (6.0)			
k, $N/mm^{1.5}$ ($lb/in.^{1.5}$)		1.60×10^4 (4.62×10^5)				1.61×10^4 (4.63×10^5)				1.60×10^4 (4.59×10^5)			
F_m, N		529	842	1513	2206	460	1362	1964	3104	518	1016	1594	2037
(lb)		(119)	(189)	(340)	(496)	(103)	(306)	(442)	(698)	(116)	(228)	(358)	(458)
α_m, 10^{-2}mm		10.3	14.0	20.7	26.6	9.40	19.3	24.6	30.1	10.2	16.0	21.5	25.3
(10^{-3} in.)		(4.05)	(5.52)	(8.16)	(10.5)	(3.69)	(7.59)	(9.69)	(11.9)	(4.01)	(6.28)	(8.48)	(9.98)
α_0, 10^{-2} mm	Area Fit	1.24	3.38	4.27	7.70	0.30	3.12	6.71	9.42	1.17	2.49	6.53	8.69
(10^{-3} in.)		(0.49)	(1.33)	(1.68)	(3.03)	(0.12)	(1.23)	(2.64)	(3.71)	(0.46)	(0.98)	(2.57)	(3.42)
	α_{cr} Fit	0.56	1.70	5.13	8.53	0.0	4.37	7.34	10.6	0.0	2.64	5.59	7.77
		(0.22)	(0.67)	(2.02)	(3.36)	(0.0)	(1.72)	(2.89)	(4.18)	(0.0)	(1.04)	(2.20)	(3.06
Area,	Area	137	256	712	1194	119	628	1016	1570	133	390	683	970
10^{-2} mm-N	Fit	(121)	(227)	(630)	(1057)	(105)	(556)	(890)	(1390)	(118)	(346)	(605)	(859)
(10^{-4} in.-lb)	α_{cr}	155	296	674	1142	123	581	969	1481	150	387	726	1024
	Fit	(137)	(262)	(596)	(1011)	(109)	(514)	(858)	(1311)	(133)	(342)	(643)	(906)

Table 4-Values of α_o and area under unloading curve by different fits for graphite/epoxy with 6.35 mm (0.25 in.) indentor

Span, mm (in.)		50.8 (2.0)						101.6 (4.0)					
Width, mm (in.)		25.4 (1.0)			38.1 (1.5)			25.4 (1.0)			38.1 (1.5)		
k, $N/mm^{1.5}$ ($lb/in.^{1.5}$)		2.06×10^4 (5.92×10^5)			1.85×10^4 (5.33×10^5)			1.83×10^4 (5.28×10^5)			2.32×10^4 (6.68×10^5)		
F_m, N (lb)		668 (150)	934 (210)	1223 (275)	273 (61.3)	561 (126)	997 (224)	408 (91.7)	612 (138)	844 (190)	277 (62.3)	662 (149)	1210 (272)
α_m, 10^{-2}mm (10^{-3} in.)		10.2 (4.01)	12.7 (5.01)	15.2 (6.00)	6.00 (2.37)	9.70 (3.83)	14.2 (5.61)	7.90 (3.12)	10.4 (4.08)	12.9 (5.06)	5.20 (2.06)	9.30 (3.68)	14.0 (5.50)
α_o, 10^{-2}mm (10^{-3}in.)	Area Fit	0.94 (0.37)	1.80 (0.71)	2.79 (1.10)	0.05 (0.02)	0.43 (0.17)	2.13 (0.84)	0.00 (0.00)	0.41 (0.16)	1.55 (0.61)	0.00 (0.00)	0.61 (0.24)	1.85 (0.73)
	α_{cr} Fit	0.91 (0.36)	2.13 (0.84)	3.45 (1.36)	0.00 (0.00)	0.71 (0.28)	2.92 (1.15)	0.00 (0.00)	1.02 (0.40)	2.21 (0.87)	0.00 (0.00)	0.56 (0.22)	2.77 (1.09
Area 10^{-2} mm - N (10^{-4} in.-lb)	Area Fit	188 (166)	291 (258)	435 (385)	46.5 (41.2)	149 (132)	345 (305)	92.2 (81.6)	174 (154)	272 (241)	41.4 (36.7)	165 (146)	418 (370)
	α_{cr} Fit	177 (156)	282 (250)	412 (365)	46.9 (41.5)	144 (128)	323 (286)	92.2 (81.6)	164 (145)	257 (227)	41.4 (36.7)	166 (147)	387 (342)

Table 5-Values of α_o and area under unloading curve by different fits for graphite/epoxy with 12.7 mm (0.5 in.) indentor

Span, mm (in.)		50.8 (2.0)						101.6 (4.0)					
Width, mm (in.)		25.4 (1.0)			38.1 (1.5)			25.4 (1.0)			38.1 (1.5)		
k, $N/mm^{1.5}$ ($lb/in.^{1.5}$)		3.56×10^4 (10.24×10^5)			3.31×10^4 (9.53×10^5)			3.18×10^4 (9.15×10^5)			3.60×10^4 (10.37×10^5)		
F_m, N		425	955	1479	719	1320	1645	227	791	1239	267	900	1285
(lb)		(95.5)	(215)	(333)	(162)	(279)	(370)	(51)	(178)	(279)	(60.1)	(202)	(289)
α_m, 10^{-2} mm		5.10	9.00	12.0	7.80	11.7	13.5	3.70	8.50	1.15	3.80	8.60	10.8
(10^{-3} in)		(2.01)	(3.53)	(4.73)	(3.07)	(4.60)	(5.32)	(1.46)	(3.35)	(4.53)	(1.50)	(3.37)	(4.27)
α_o, 10^{-2} mm	Area	0.00	0.76	2.18	0.03	1.30	2.31	0.05	0.56	1.65	0.00	0.03	1.35
	Fit	(0.00)	(0.30)	(0.86)	(0.01)	(0.51)	(0.91)	(0.02)	(0.22)	(0.65)	(0.00)	(0.01)	(0.53)
(10^{-3} in)	α_{cr}	0.00	0.38	1.78	0.00	1.68	2.51	0.00	0.20	1.55	0.00	0.20	1.22
	Fit	(0.00)	(0.15)	(0.70)	(0.00)	(0.66)	(0.99)	(0.00)	(0.08)	(0.61)	(0.00)	(0.08)	(0.48)
Area,	Area	63.4	224	415	159	392	527	23.7	180	349	29.0	220	348
	Fit	(56.1)	(198)	(367)	(141)	(347)	(466)	(20.9)	(159)	(309)	(25.7)	(194)	(308)
10^{-2} mm - N	α_{cr}	63.4	234	432	160	379	516	24.0	188	353	29.0	214	353
(10^{-4}in.-lb)	Fit	(56.1)	(207)	(382)	(142)	(335)	(457)	(21.2)	(166)	(312)	(25.7)	(190)	(312)

Table 6-Comparison of loading rigidity k and reloading rigidity k_1 for graphite/epoxy with 12.7 mm (0.5 in.) indentor

Span, mm (in.)	50.8 (2.0)			101.6 (4.0)					
Width, mm (in.)	25.4 (1.0)			25.4 (1.0)			38.1 (1.5)		
k, $N/mm^{1.5}$ ($lb/in.^{1.5}$)	3.56×10^4 (10.24×10^5)			3.18×10^4 (9.15×10^5)			3.60×10^4 (10.37×10^5)		
F_m, N (lb)	428 (95)	955 (215)	1479 (333)	227 (51)	791 (178)	1239 (279)	267 (60)	900 (202)	1285 (289)
α_m, 10^{-2} mm (10^{-3} in.)	5.11 (2.01)	8.97 (3.53)	12.0 (4.73)	3.71 (1.46)	8.51 (3.35)	11.5 (4.53)	3.81 (1.5)	8.56 (3.37)	10.8 (4.27)
α_o, 10^{-2} mm (10^{-3} in.)	0.0 (0.0)	0.76 (0.30)	2.18 (0.86)	0.05 (0.02)	0.56 (0.22)	1.65 (0.65)	0.0 (0.0)	0.25 (0.01)	1.35 (0.53)
k_1, 10^4 $N/mm^{1.5}$ (10^5 $lb/in.^{1.5}$)	3.68 (10.6)	4.06 (11.7)	4.80 (13.8)	3.24 (9.33)	3.53 (10.2)	4.01 (11.5)	3.59 (10.3)	3.61 (10.4)	3.67 (10.6)

Table 7-Values of k' for graphite/epoxy (Equation (19)).

Ball Diameter mm (in.)	6.35 (0.25)				12.7 (0.50)			
Span, mm (in.)	50.8 (2.0)		101.6 (4.0)		50.8 (2.0)		101.6 (4.0)	
Width, mm (in.)	25.4 (1.0)	38.1 (1.5)	25.4 (1.0)	38.1 (1.5)	25.4 (1.0)	38.1 (1.5)	25.4 (1.0)	38.1 (1.5)
k', GPa (10^5 psi)	0.92 (1.34)	0.81 (1.18)	0.81 (1.17)	0.98 (1.42)	0.77 (1.12)	0.74 (1.08)	0.72 (1.05)	0.81 (1.17)

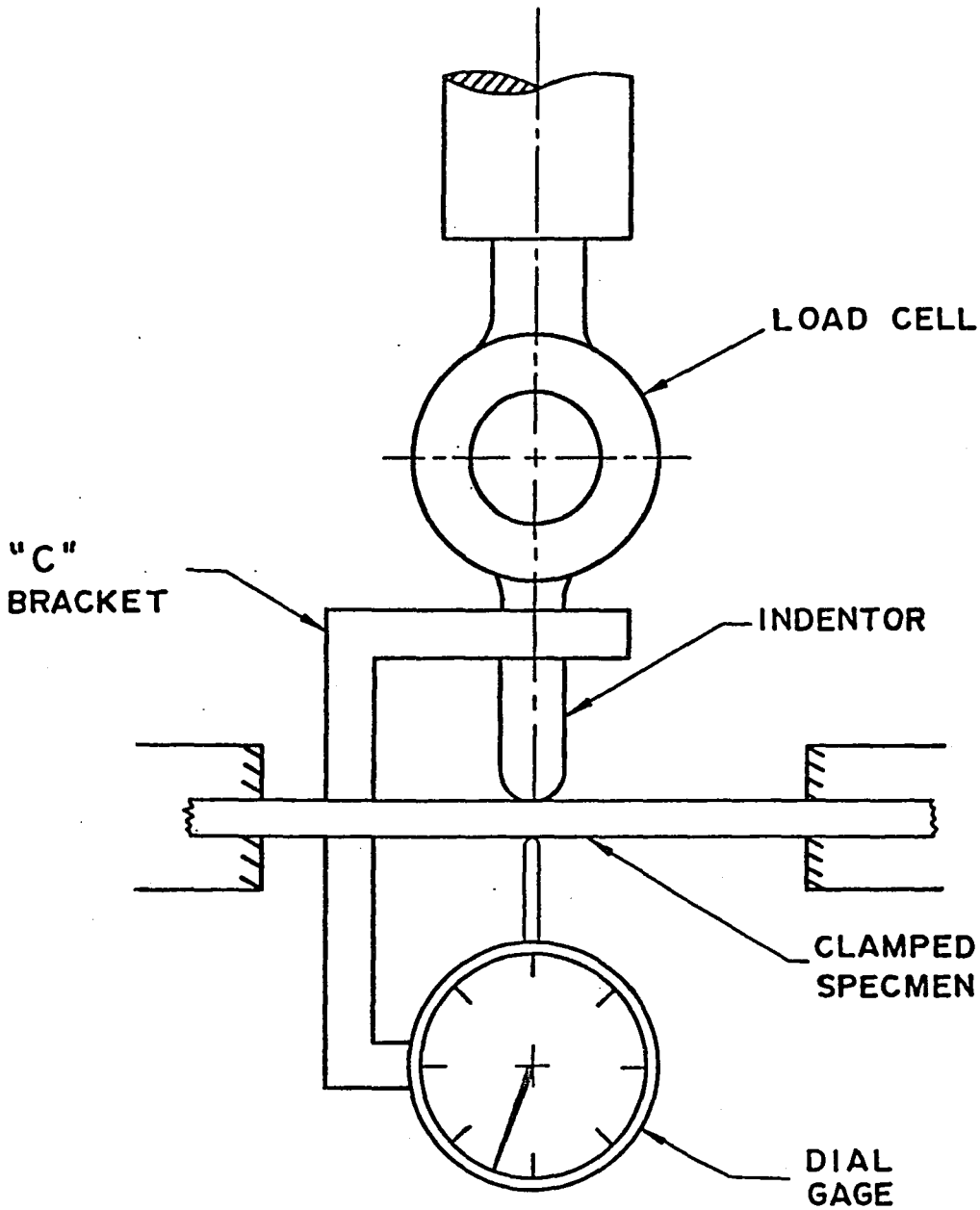

Fig. 1 Indentation test set-up

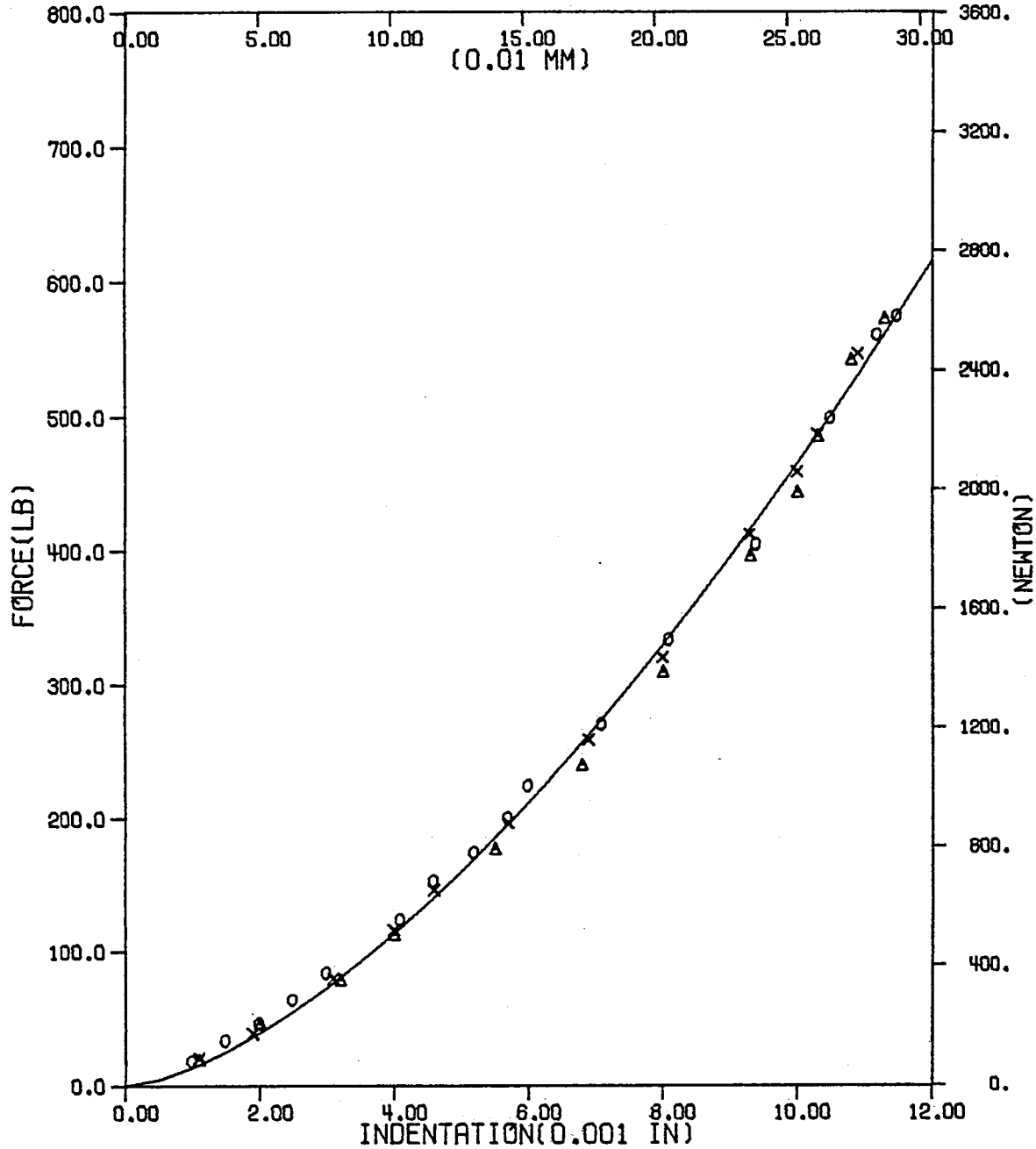

Fig. 2 - Least-square fit for loading for glass/epoxy with 50.8 mm(2")-span and 6.35 mm (0.25") diameter indentor.

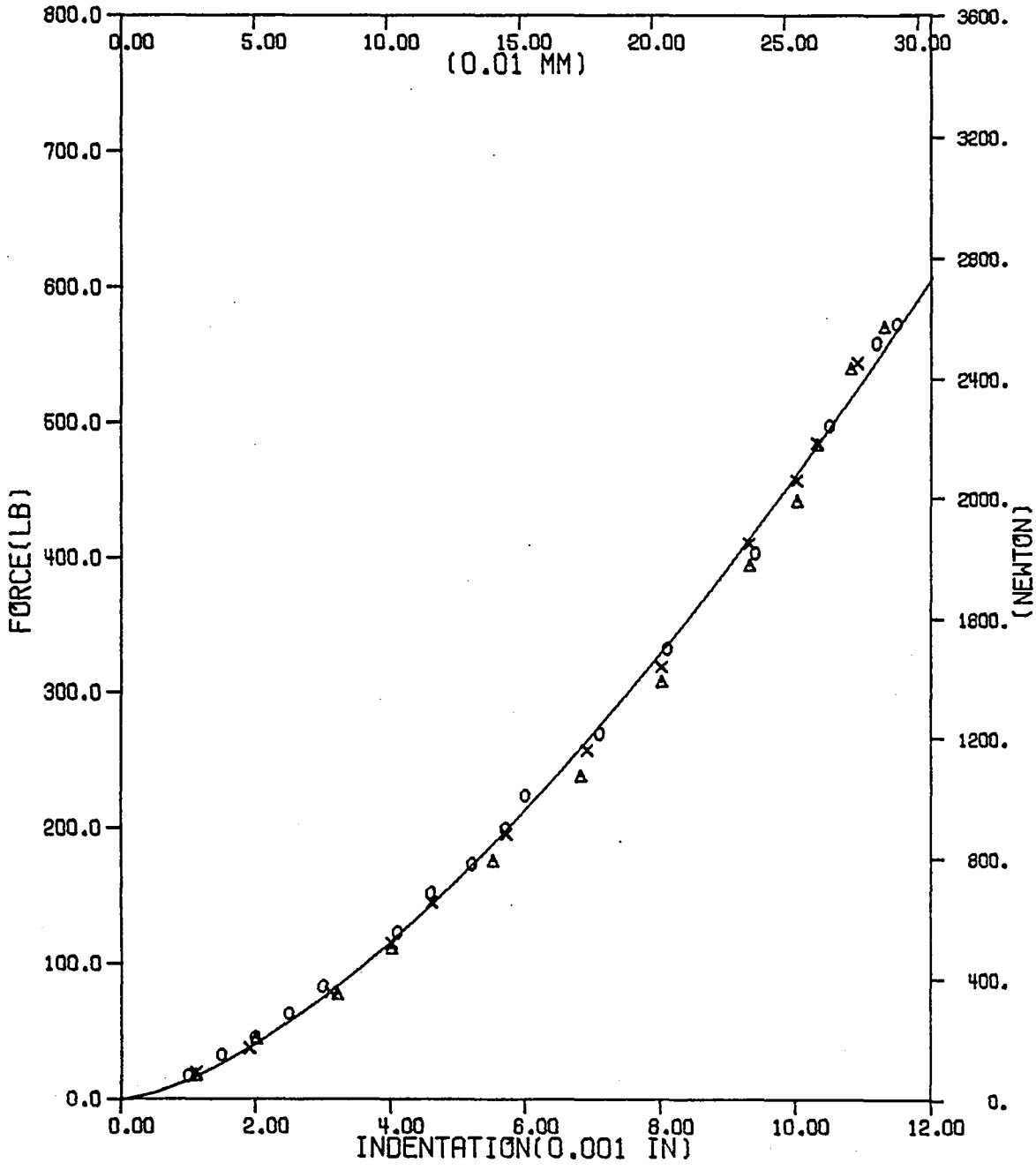

Fig. 3 - Least-square fit for loading with n = 1.5 for glass/epoxy with 50.8 mm(2")-span and 6.35 mm(0.25") diameter indentor.

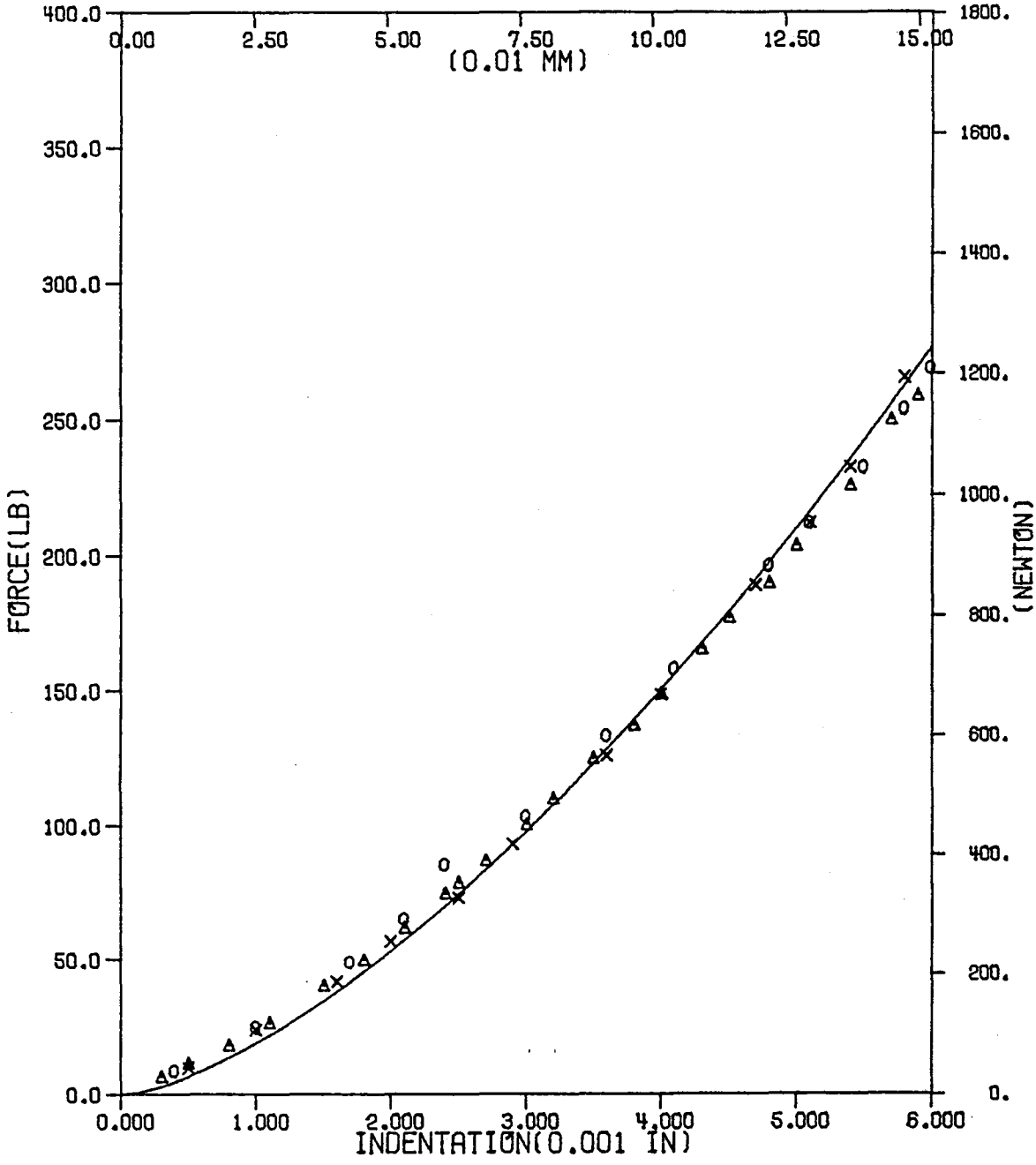

Fig. 4 - Least-square fit for loading with n = 1.5 for graphite/epoxy with 50.8 mm(2")-span 25.4 mm-width, and 6.35 mm (0.25") indentor.

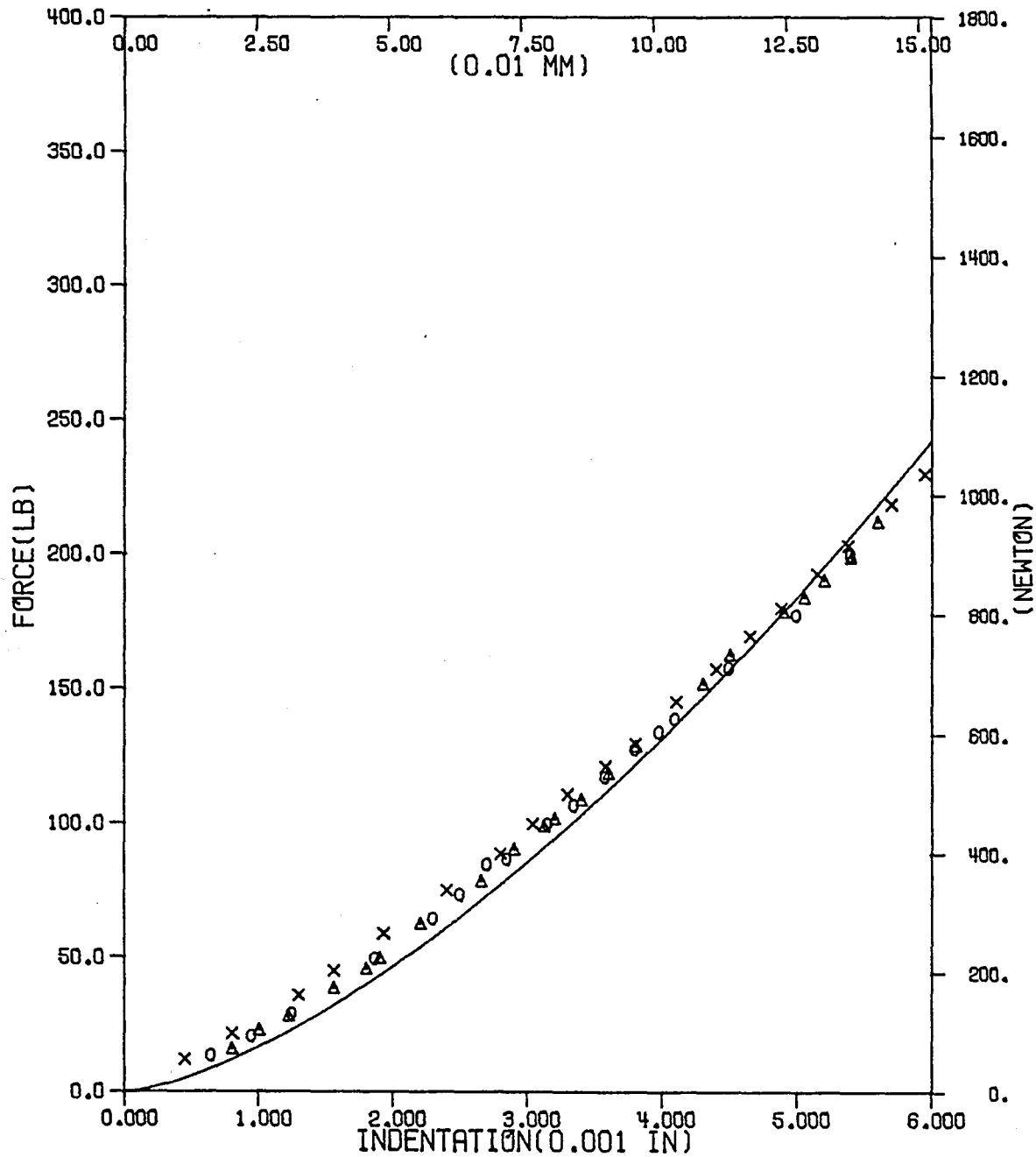

Fig. 5 - Least-square fit for loading with n = 1.5 for graphite/epoxy with 101.6 mm(4")-span, 25.4 mm-width, and 6.35 mm(0.25") indentor.

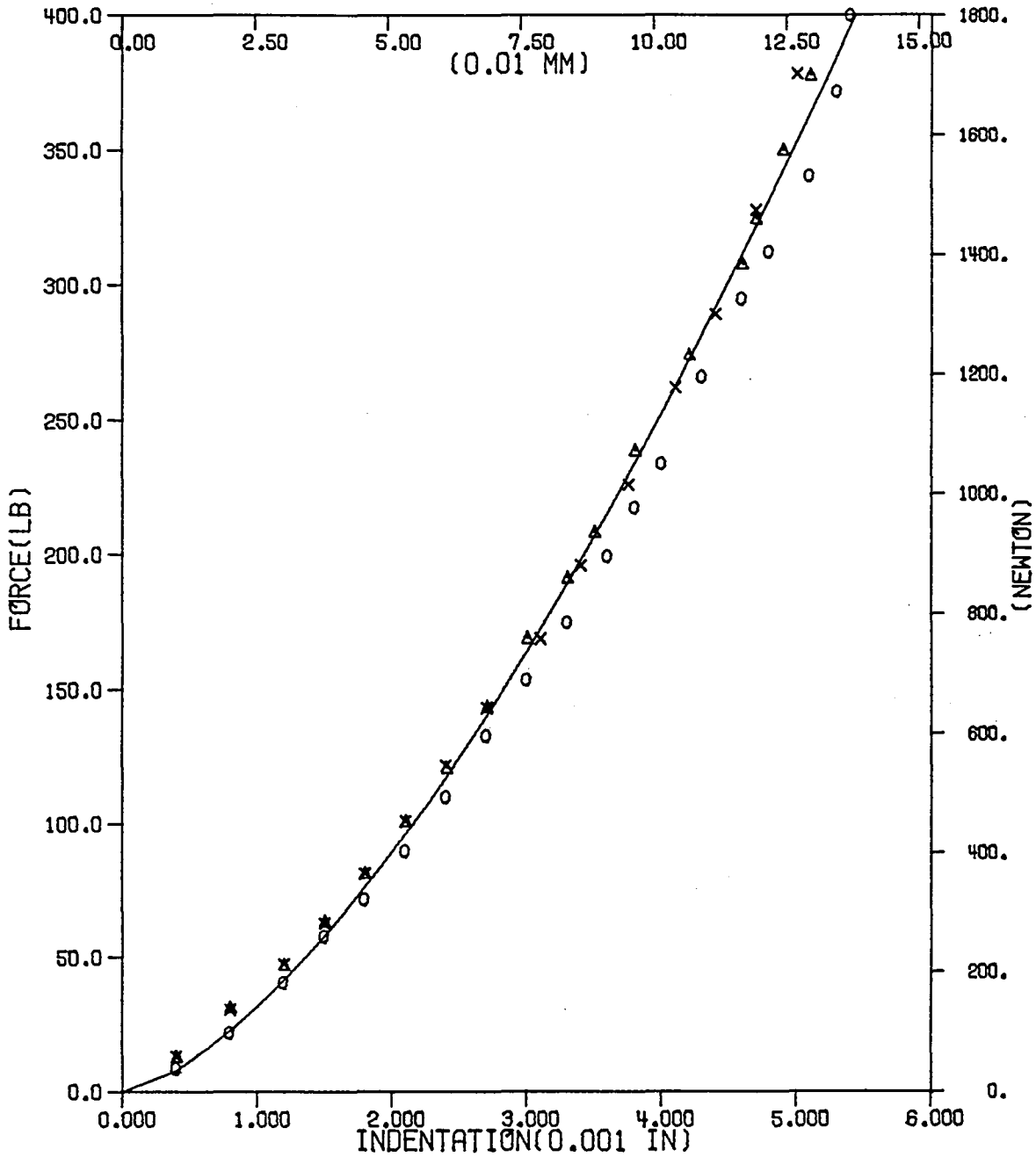

Fig. 6 - Least-square fit for loading with n = 1.5 for graphite/epoxy with 50.8 mm(2")-span, 25.4 mm(1")-width, and 12.7 mm(0.5") indentor.

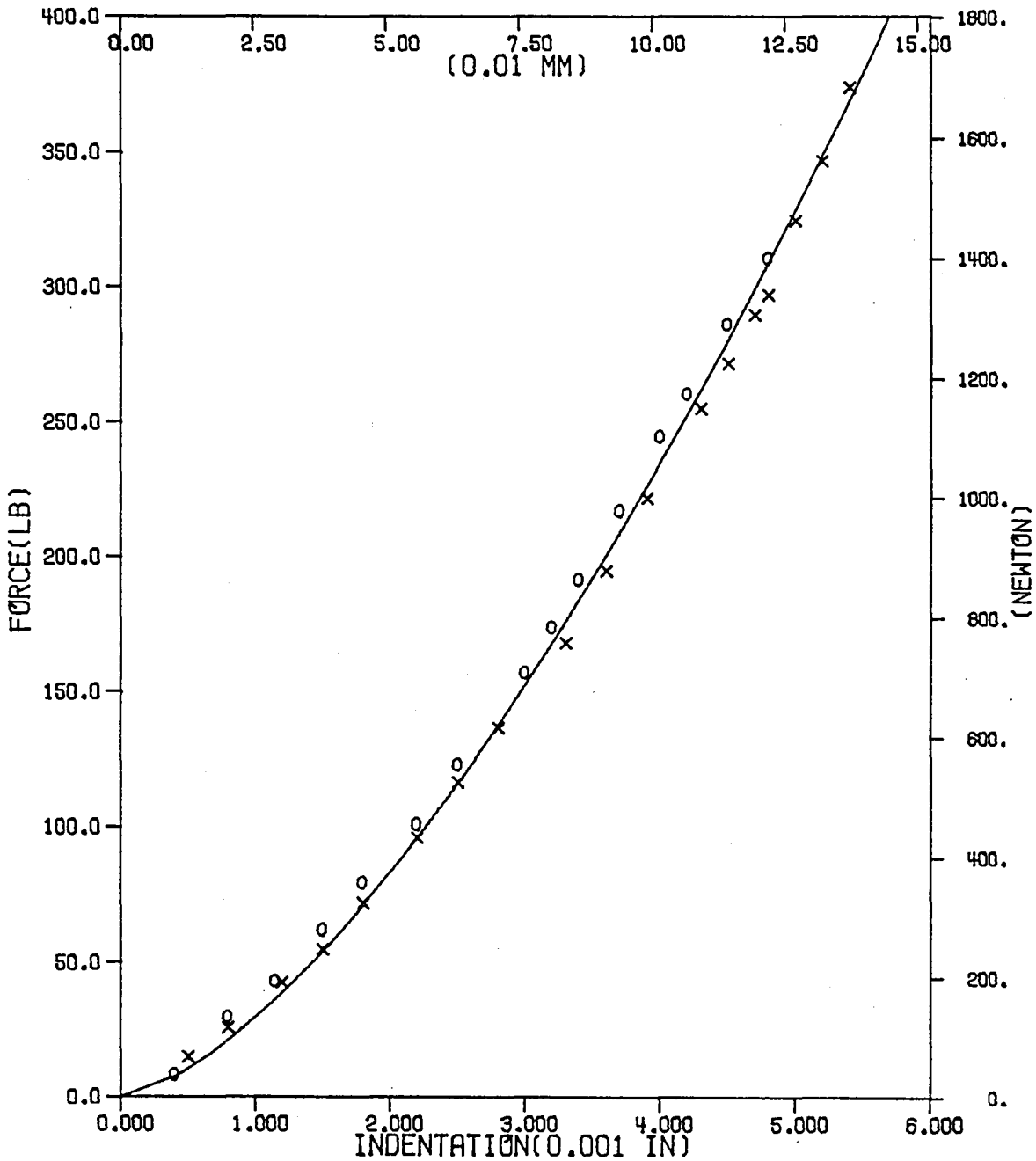

Fig. 7 - Least-square fit for loading with n = 1.5 for graphite/epoxy with 101.6 mm(4")-span, 25.4 mm(1")-width, and 12.7 mm(0.5") indentor.

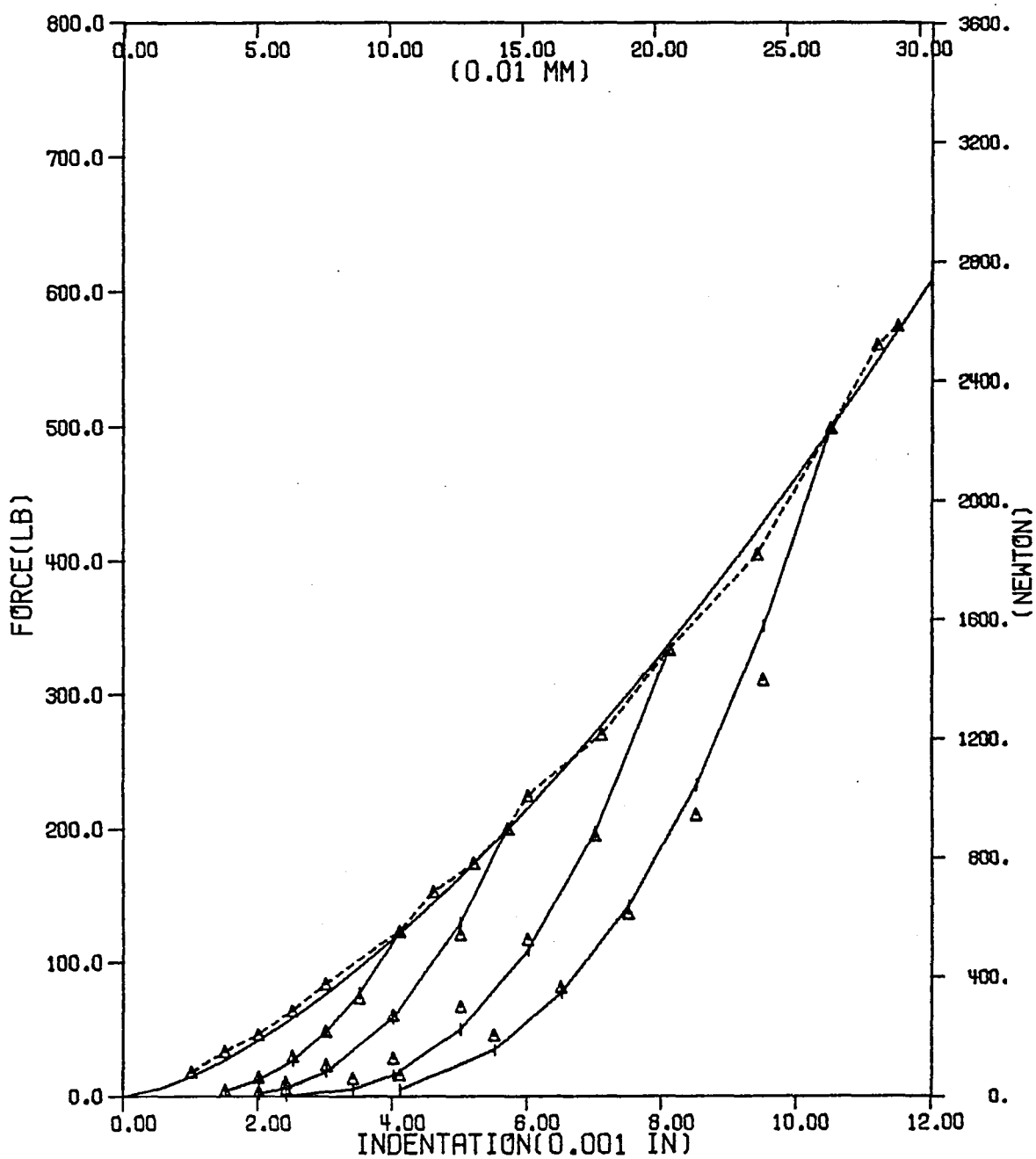

Fig. 8 - Unloading curves for glass/epoxy with q = 2.5, 50.8 mm(2")-span and 6.35 mm(0.25") indentor.

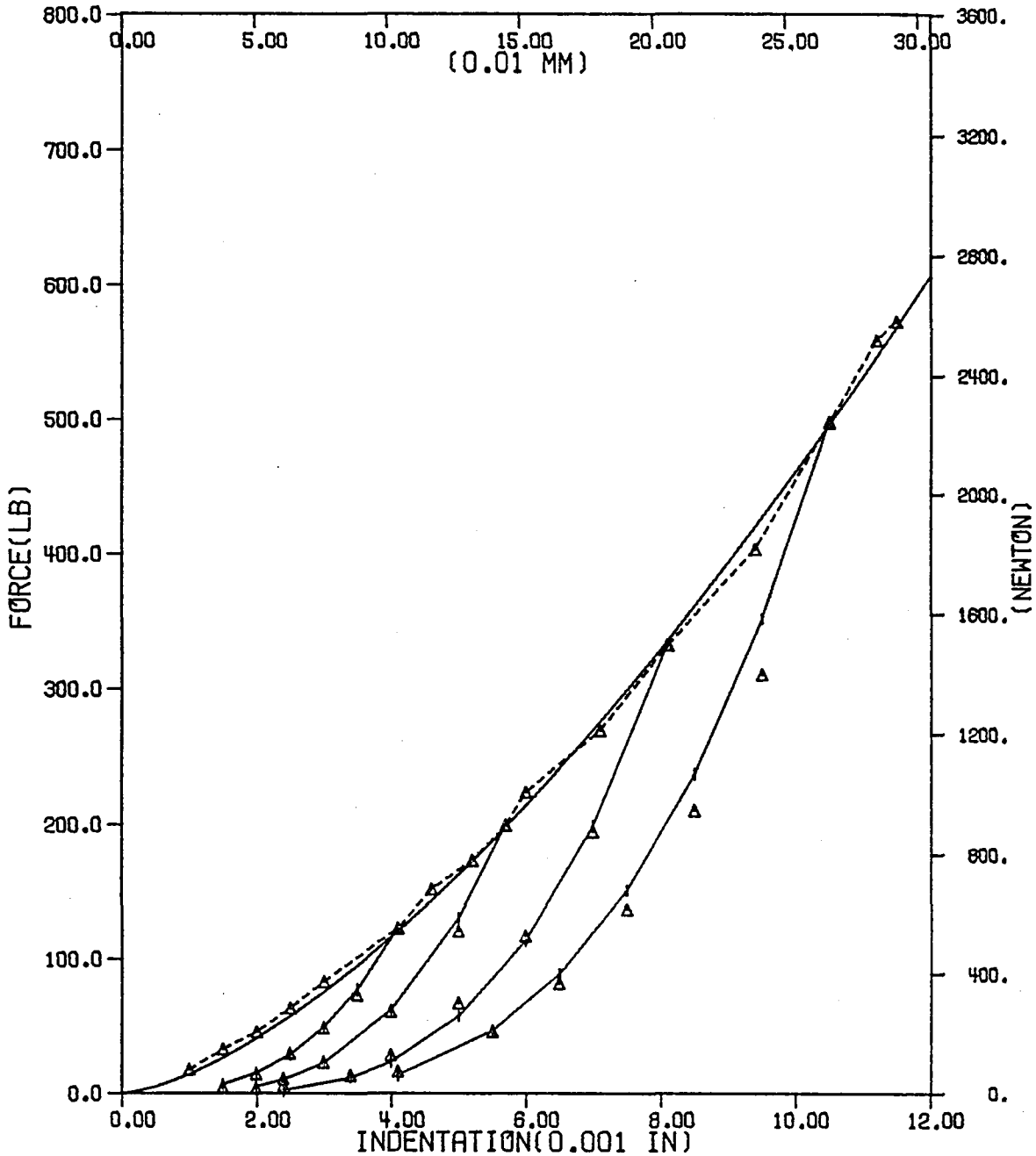

Fig. 9 - Unloading curves for glass/epoxy with q = 3.0, 50.8 mm(2")-span, and 6.35 mm(0.25") indentor.

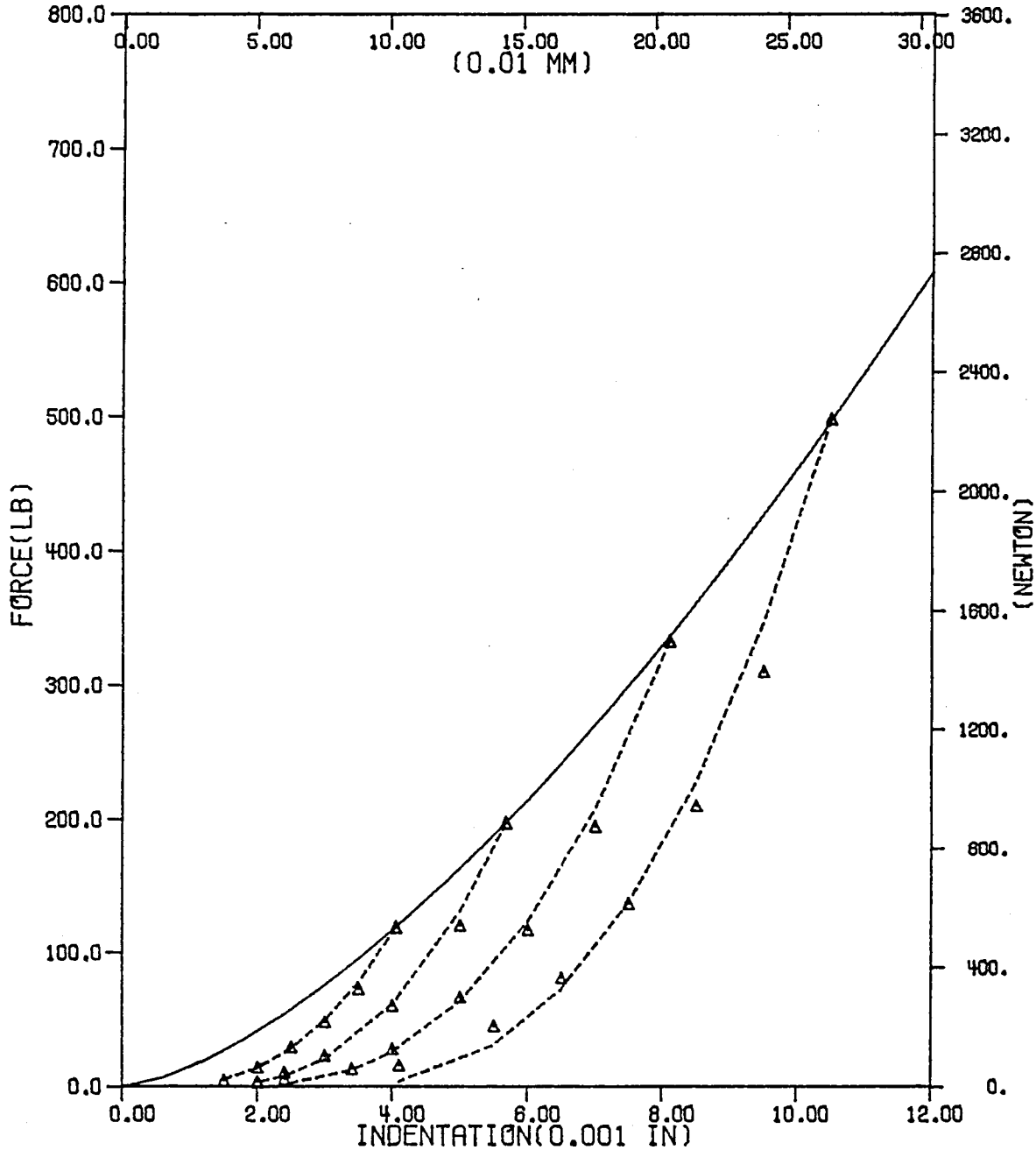

Fig. 10 - Unloading curves for glass/epoxy with 50.8 mm(2")-span and 6.35 mm(0.25) indentor using area fit.

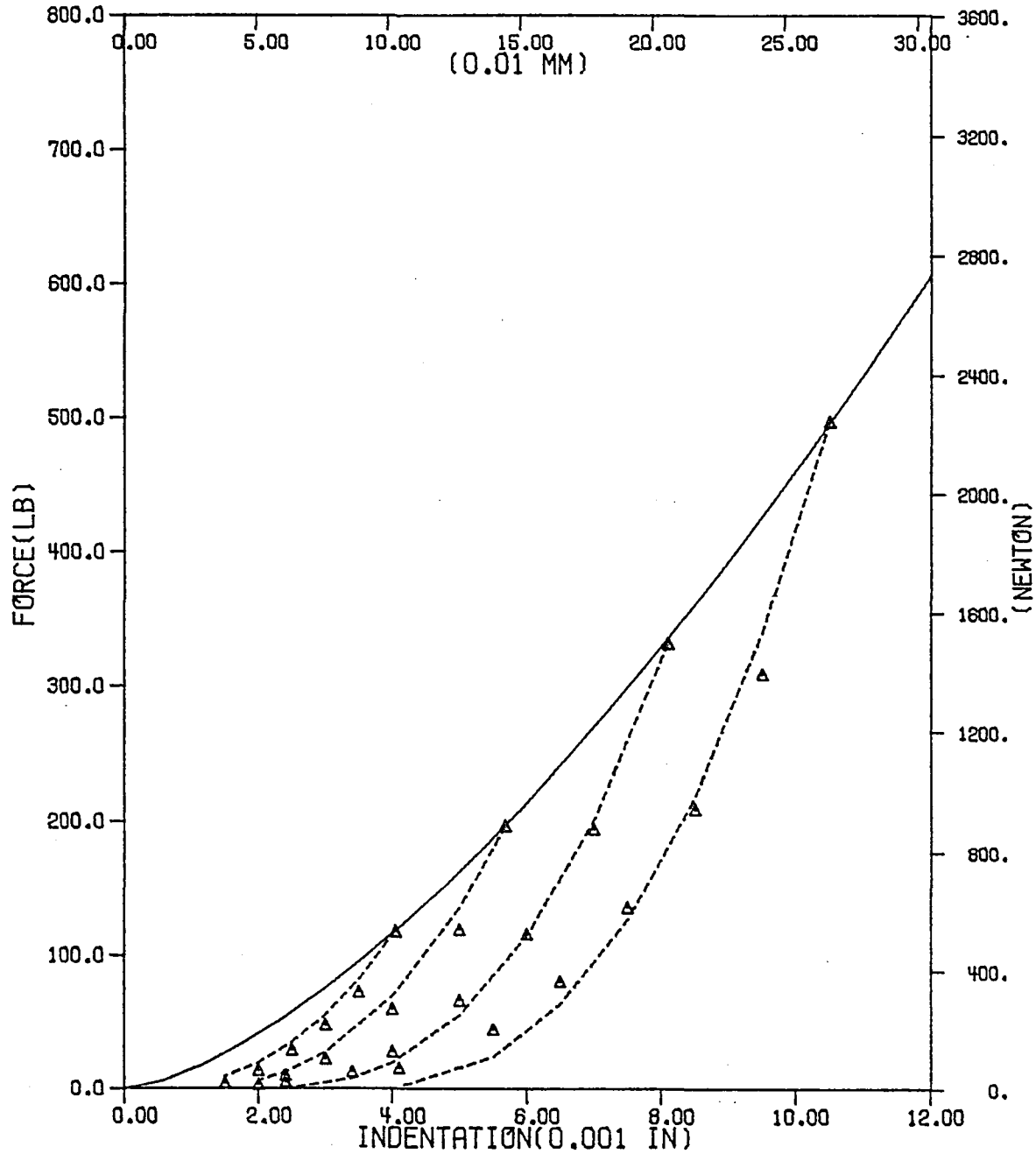

Fig. 11 - Unloading curves for glass/epoxy with 50.8 mm(2")-span and 6.35 mm(0.25") indentor using α_{cr} = 0.102 mm(0.004").

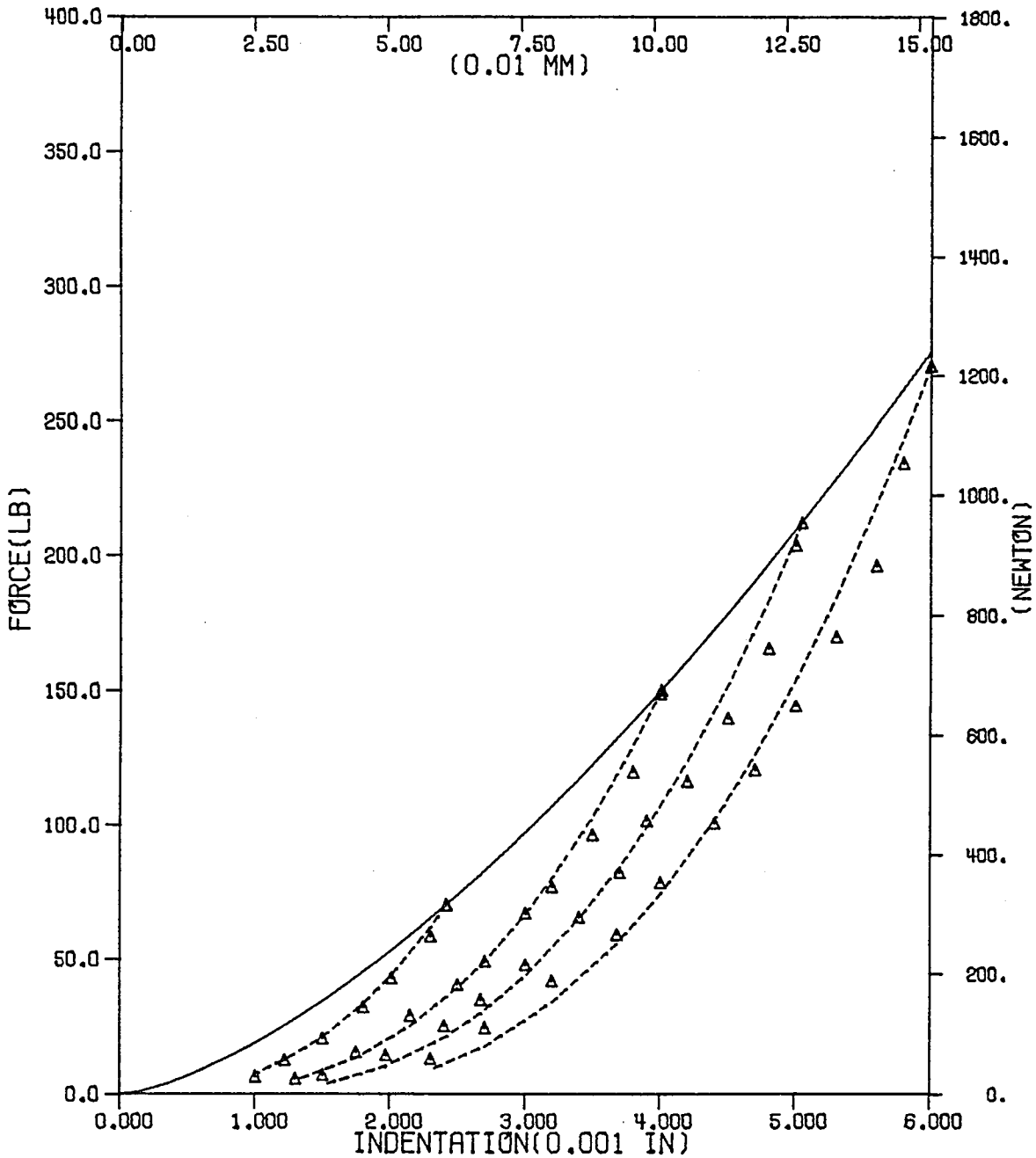

Fig. 12 - Unloading curves for graphite/epoxy with 50.8 mm(2")-span, 25.4 mm(1")-width and 6.35 mm(0.25") indentor using area fit.

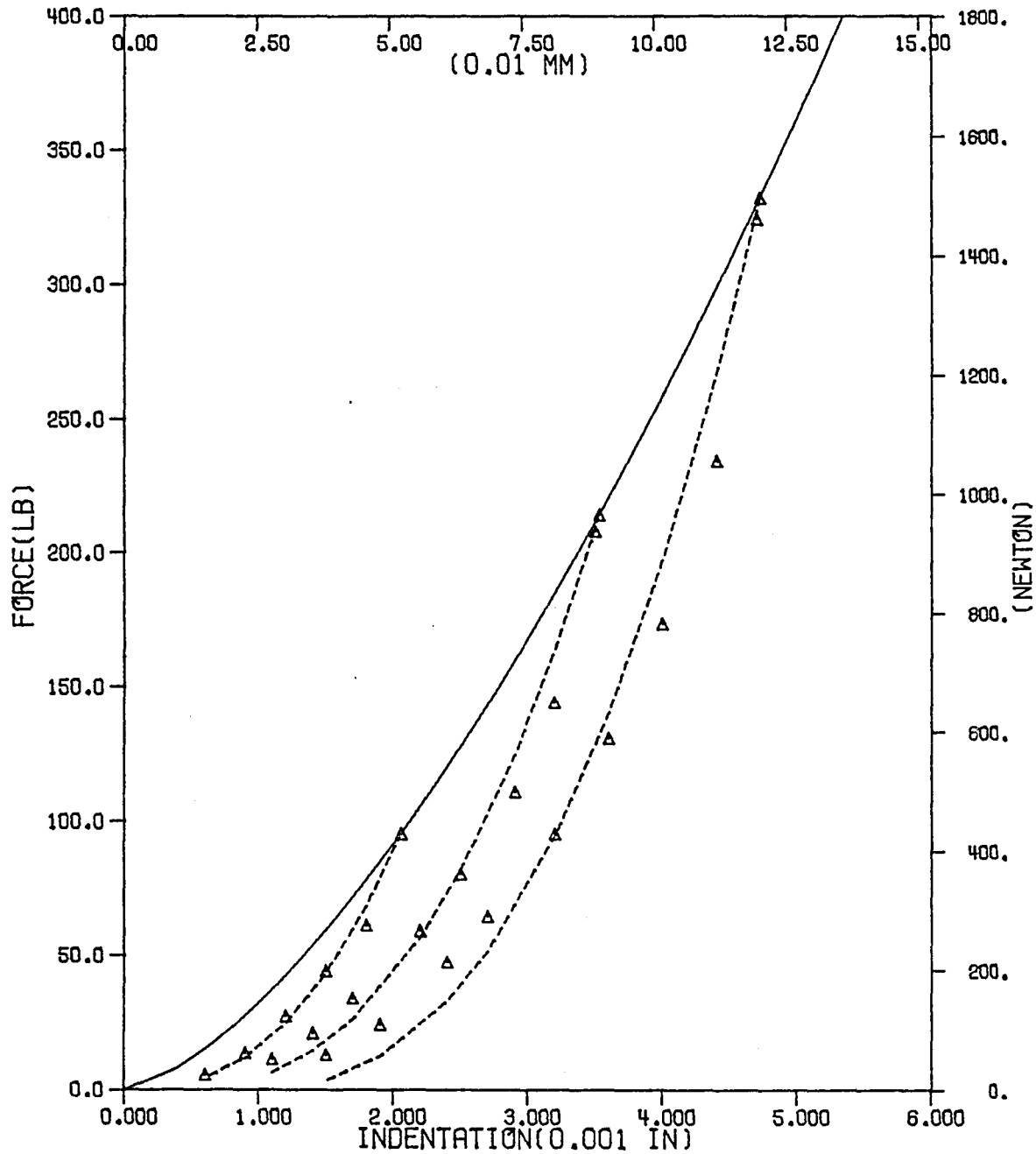

Fig. 13 - Unloading curves for graphite/epoxy with 50.8 mm(2")-span, 25.4 mm(1")-width, and 12.7 mm(0.5") indentor using area fit.

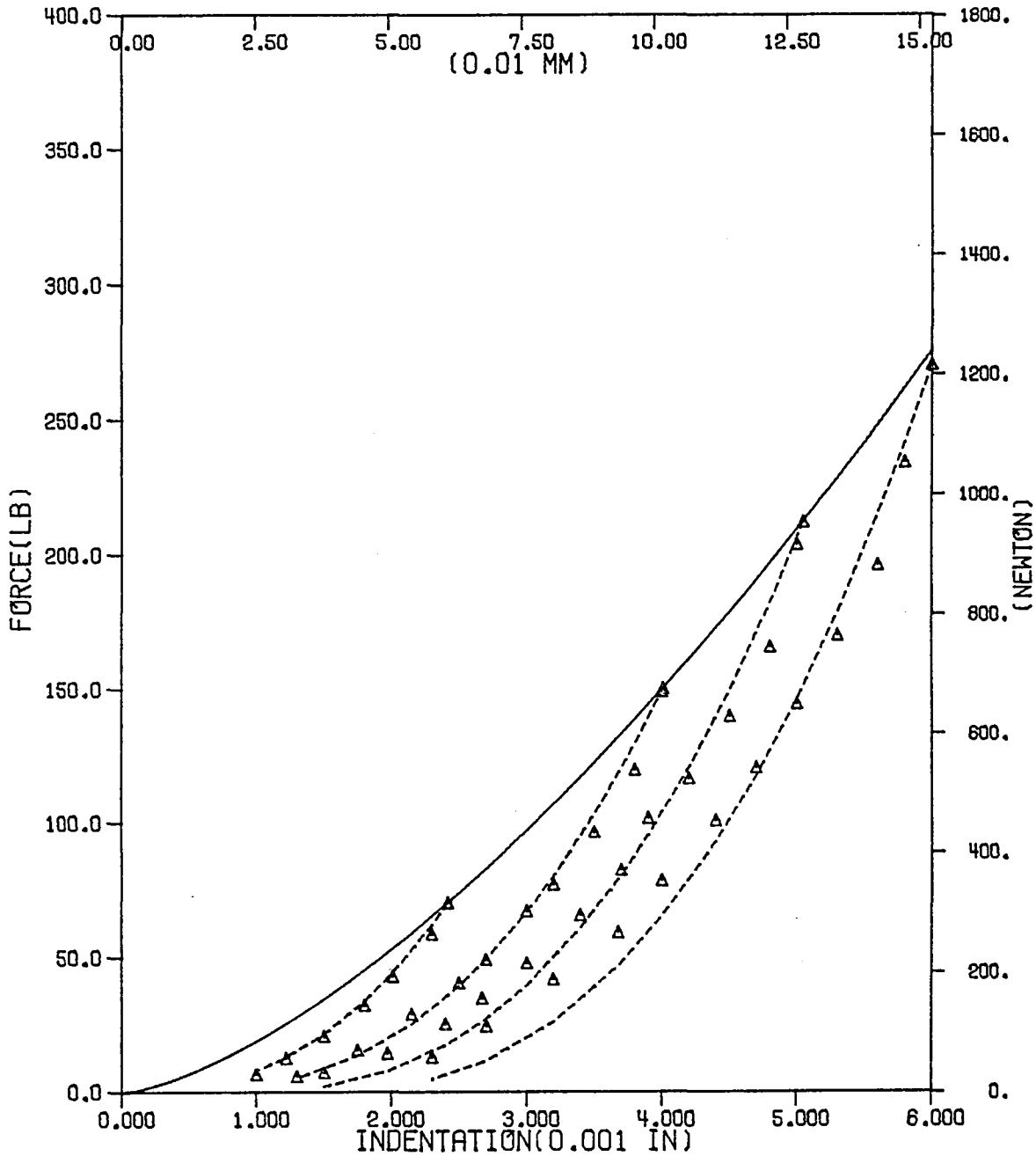

Fig. 14 - Unloading curves for graphite/epoxy with 50.8 mm(2")-span, 25. mm(1")-width, and 6.35 mm(0.25") indentor using α_{cr} = 0.0803 mm(0.00316").

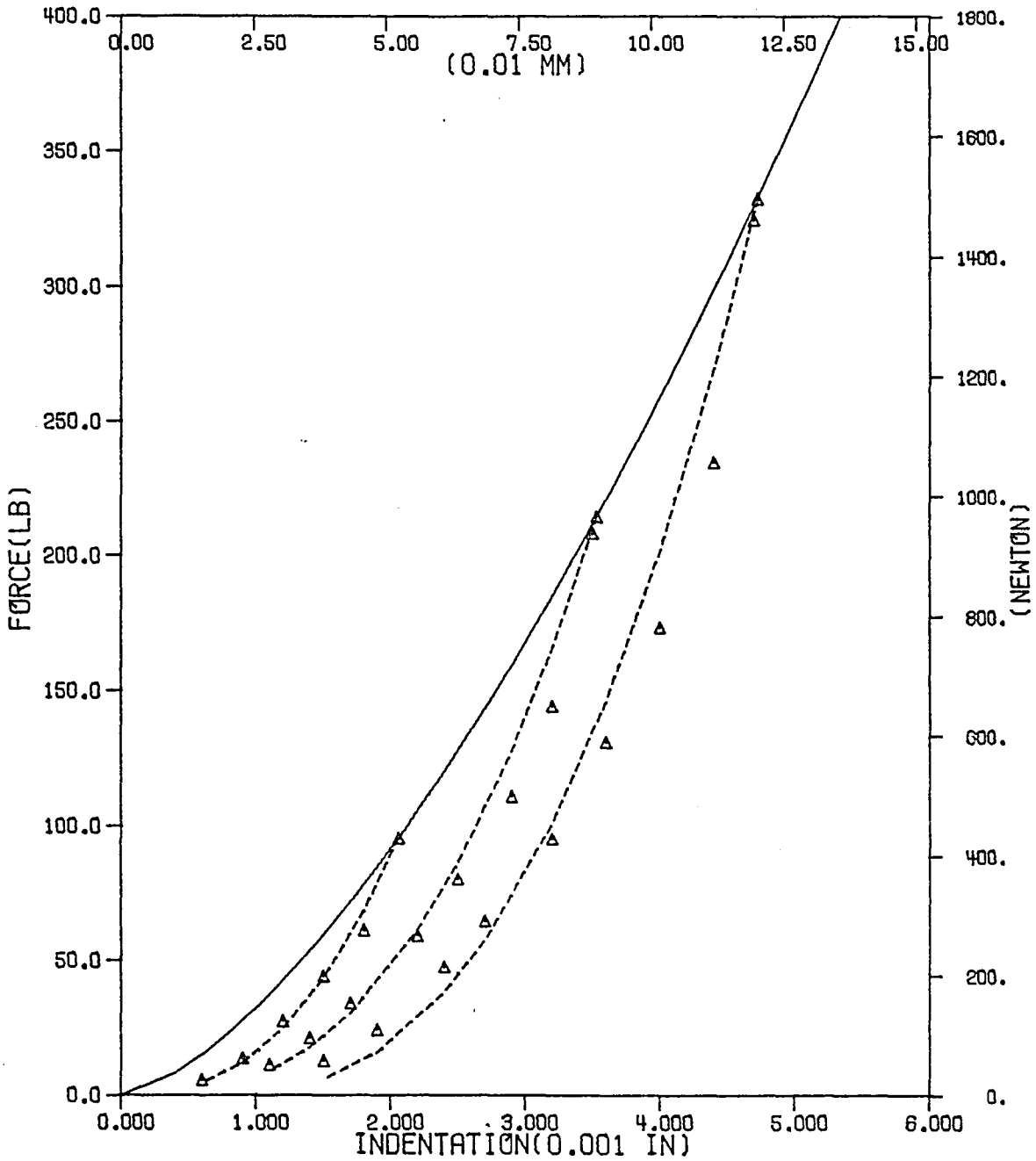

Fig. 15 - Unloading curves for graphite/epoxy with 50.8 mm(2")-span, 25.4 mm(1")-width, and 12.7 mm(0.5") indentor using α_{cr} = 0.0803 mm (0.00316").

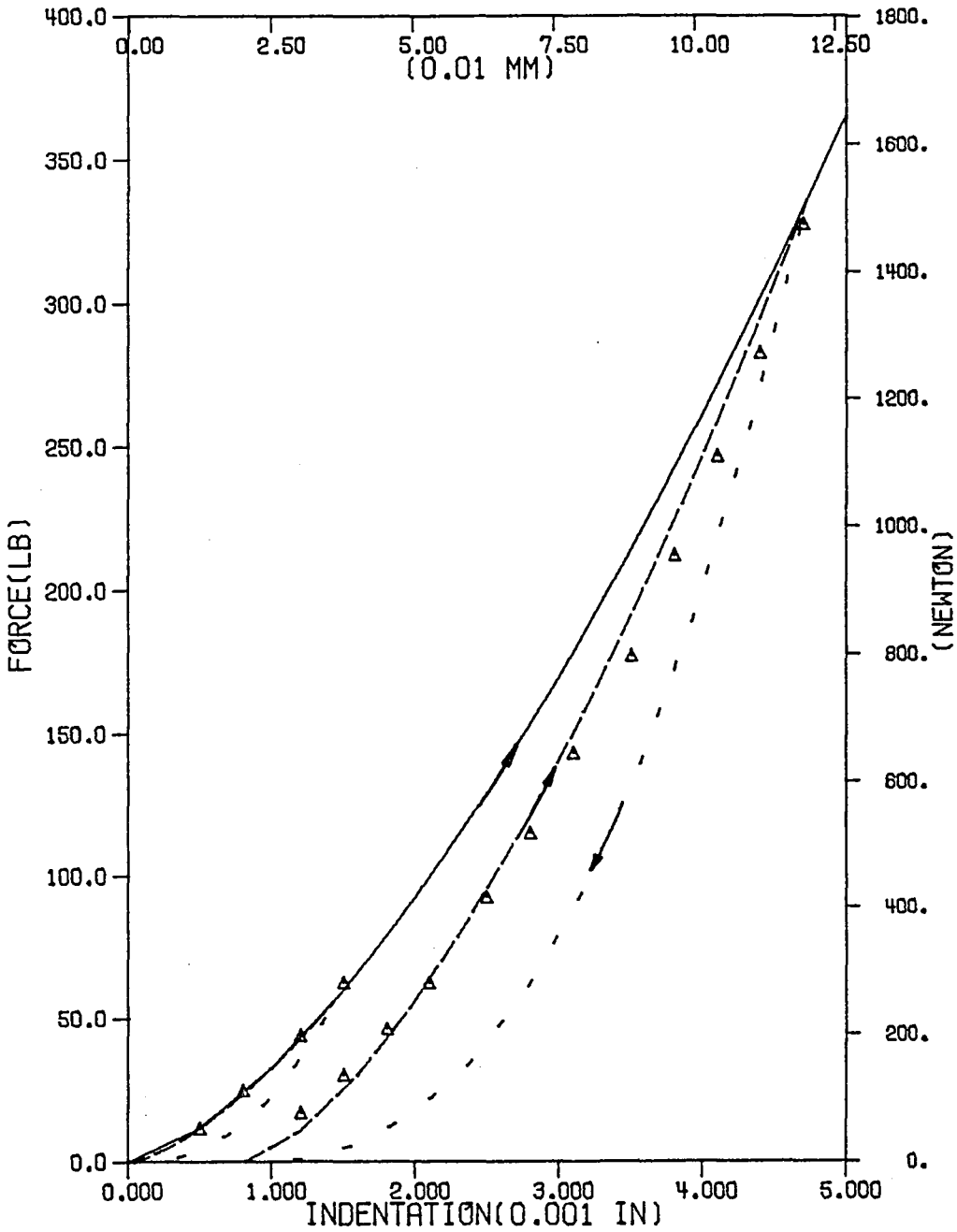

Fig. 16 - Reloading curves for graphite/epoxy with 50.8 mm(2")-span and 12.7 mm (0.5") indentor.

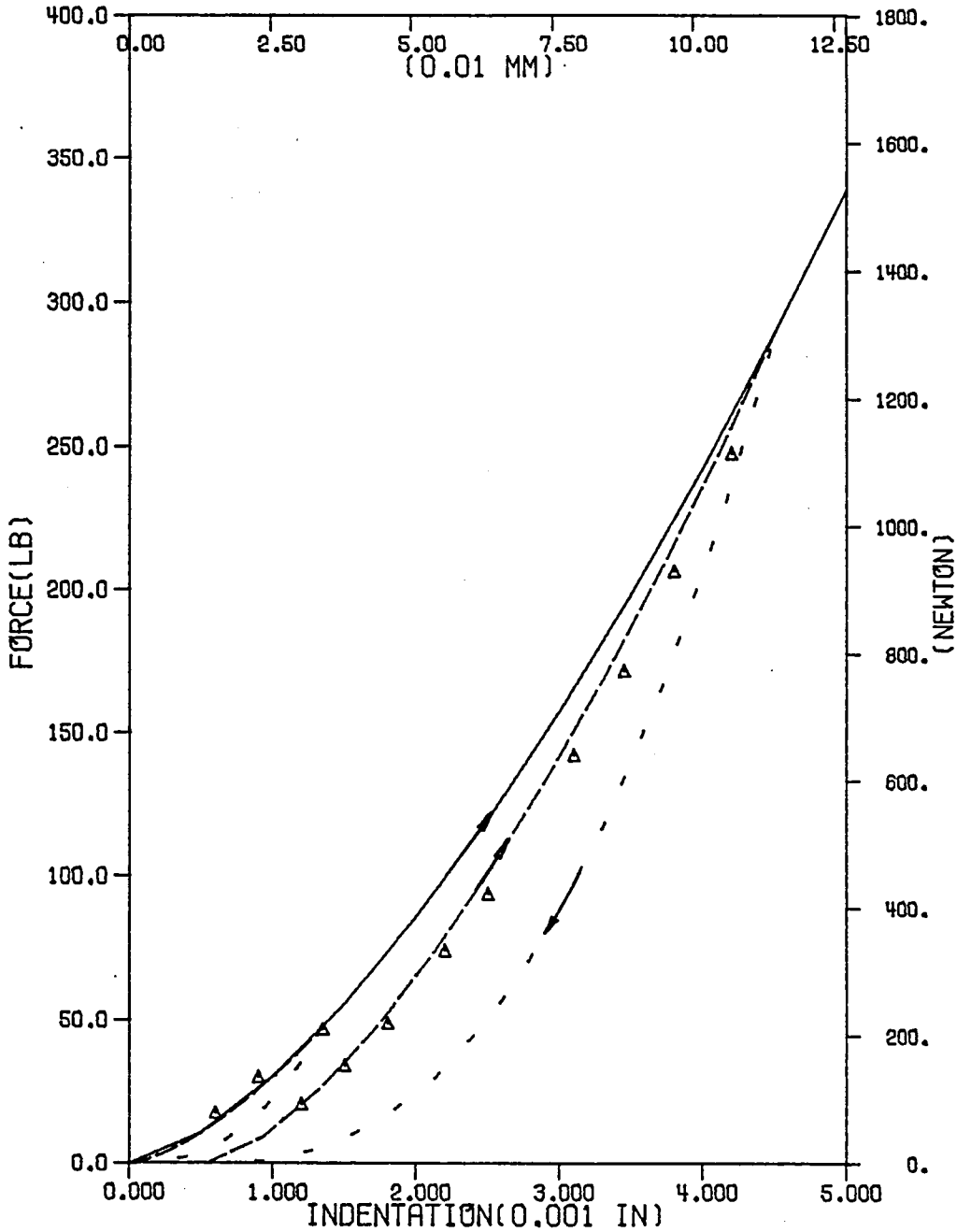

Fig. 17 - Reloading curves for graphite/epoxy with 101.6 mm(4")-span and 12.7 mm(0.5") indentor.

TOPICAL REPORT

NSG-3185

INDENTATION LAW FOR COMPOSITE LAMINATES

NASA CR-165460

Advanced Research Projects Agency
Washington DC 20525
Attn: Library

Advanced Technology Center, Inc.
LTV Aerospace Corporation
P.O. Box 6144
Dallas, TX 75222
Attn: D. H. Petersen
W. J. Renton

Air Force Flight Dynamics Laboratory
Wright-Patterson Air Force Base, OH 45433
Attn: E. E. Baily
G. P. Sendeckyj (FBC)
R. S. Sandhu

Air Force Materials Laboratory
Wright-Patterson Air Force Base, OH 45433
Attn: H. S. Schwartz (LN)
T. J. Reinhart (MBC)
G. P. Peterson (LC)
E. J. Morrisey (LAE)
S. W. Tsai (MBM)
N. J. Pagano
J. M. Whitney (MBM)

Air Force Office of Scientific Research
Washington DC 20333
Attn: J. F. Masi (SREP)

Air Force Office of Scientific Research
1400 Wilson Blvd.
Arlington, VA 22209

AFOSR/NA
Bolling AFB, DC 20332
Attn: A. K. Amos

Air Force Rocket Propulsion Laboratory
Edwards, CA 93523
Attn: Library

Babcock & Wilcox Company
Advanced Composites Department
P.O. Box 419
Alliance, Ohio 44601
Attn: P. M. Leopold

Bell Helicopter Company
P.O. Box 482
Ft. Worth, TX 76101
Attn: H. Zinberg

The Boeing Company
P. O. Box 3999
Seattle, WA 98124
Attn: J. T. Hoggatt, MS. 88-33
T. R. Porter

The Boeing Company
Vertol Division
Morton, PA 19070
Attn: E. C. Durchlaub

Battelle Memorial Institute
Columbus Laboratories
505 King Avenue
Columbus, OH 43201
Attn: L. E. Hulbert

Bendix Advanced Technology Center
9140 Old Annapolis Rd/Md. 108
Columbia, MD 21045
Attn: O. Hayden Griffin

Brunswick Corporation
Defense Products Division
P. O. Box 4594
43000 Industrial Avenue
Lincoln, NE 68504
Attn: R. Morse

Celanese Research Company
86 Morris Ave.
Summit, NJ 07901
Attn: H. S. Kliger

Commander
Natick Laboratories
U. S. Army
Natick, MA 01762
Attn: Library

Commander
Naval Air Systems Command
U. S. Navy Department
Washington DC 20360
Attn: M. Stander, AIR-43032D

Commander
Naval Ordnance Systems Command
U.S. Navy Department
Washington DC 20360
Attn: B. Drimmer, ORD-033
M. Kinna, ORD-033A

Cornell University
Dept. Theoretical & Applied Mech.
Thurston Hall
Ithaca, NY 14853
Attn: S. L. Phoenix

Defense Metals Information Center
Battelle Memorial Institute
Columbus Laboratories
505 King Avenue
Columbus, OH 43201

Department of the Army
U.S. Army Aviation Materials Laboratory
Ft. Eustis, VA 23604
Attn: I. E. Figge, Sr.
Library

Department of the Army
U.S. Army Aviation Systems Command
P.O. Box 209
St. Louis, MO 63166
Attn: R. Vollmer, AMSAV-A-UE

Department of the Army
Plastics Technical Evaluation Center
Picatinny Arsenal
Dover, NJ 07801
Attn: H. E. Pebly, Jr.

Department of the Army
Watervliet Arsenal
Watervliet, NY 12189
Attn: G. D'Andrea

Department of the Army
Watertown Arsenal
Watertown, MA 02172
Attn: A. Thomas

Department of the Army
Redstone Arsenal
Huntsville, AL 35809
Attn: R. J. Thompson, AMSMI-RSS

Department of the Navy
Naval Ordnance Laboratory
White Oak
Silver Spring, MD 20910
Attn: R. Simon

Department of the Navy
U.S. Naval Ship R&D Laboratory
Annapolis, MD 21402
Attn: C. Hersner, Code 2724

Director
Deep Submergence Systems Project
6900 Wisconsin Avenue
Washington DC 20015
Attn: H. Bernstein, DSSP-221

Director
Naval Research Laboratory
Washington DC 20390
Attn: Code 8430
I. Wolock, Code 8433

Drexel University
32nd and Chestnut Streets
Philadelphia, PA 19104
Attn: P. C. Chou

E. I. DuPont DeNemours & Co.
DuPont Experimental Station
Wilmington, DE 19898
Attn: D. L. G. Sturgeon

Fiber Science, Inc.
245 East 157 Street
Gardena, CA 90248
Attn: E. Dunahoo

General Dynamics
P.O. Box 748
Ft. Worth, TX 76100
Attn: D. J. Wilkins
Library

General Dynamics/Convair
P.O. Box 1128
San Diego, CA 92112
Attn: J. L. Christian
R. Adsit

General Electric Co.
Evendale, OH 45215
Attn: C. Stotler
R. Ravenhall

General Motors Corporation
Detroit Diesel-Allison Division
Indianapolis, IN 46244
Attn: M. Herman

Georgia Institute of Technology
School of Aerospace Engineering
Atlanta, GA 30332
Attn: L. W. Rehfield

Grumman Aerospace Corporation
Bethpage, Long Island, NY 11714
Attn: S. Dastin
J. B. Whiteside

Hamilton Standard Division
United Aircraft Corporation
Windsor Locks, CT 06096
Attn: W. A. Percival

Hercules, Inc.
Allegheny Ballistics Laboratory
P. O. Box 210
Cumberland, MD 21053
Attn: A. A. Vicario

Hughes Aircraft Company
Culver City, CA 90230
Attn: A. Knoell

Illinois Institute of Technology
10 West 32 Street
Chicago, IL 60616
Attn: L. J. Broutman

IIT Research Institute
10 West 35 Street
Chicago, IL 60616
Attn: I. M. Daniel

Jet Propulsion Laboratory
4800 Oak Grove Drive
Pasadena, CA 91103
Attn: Library

Lawrence Livermore Laboratory
P.O. Box 808, L-421
Livermore, CA 94550
Attn: T. T. Chiao
E. M. Wu

Lehigh University
Institute of Fracture &
Solid Mechanics
Bethlehem, PA 18015
Attn: G. C. Sih

Lockheed-Georgia Co.
Advanced Composites Information Center
Dept. 72-14, Zone 402
Marietta, GA 30060
Attn: T. M. Hsu

Lockheed Missiles and Space Co.
P.O. Box 504
Sunnyvale, CA 94087
Attn: R. W. Fenn

Lockheed-California
Burbank, CA 91503
Attn: J. T. Ryder
K. N. Lauraitis
J. C. Ekvall

McDonnell Douglas Aircraft Corporation
P.O. Box 516
Lambert Field, MS 63166
Attn: J. C. Watson

McDonnell Douglas Aircraft Corporation
3855 Lakewood Blvd.
Long Beach, CA 90810
Attn: L. B. Greszczuk

Material Sciences Corporation
1777 Walton Road
Blue Bell, PA 19422
Attn: B. W. Rosen

Massachusetts Institute of Technology
Cambridge, MA 02139
Attn: F. J. McGarry
J. F. Mandell
J. W. Mar

NASA-Ames Research Center
Moffett Field, CA 94035
Attn: Dr. J. Parker
Library

NASA-Flight Research Center
P.O. Box 273
Edwards, CA 93523
Attn: Library

NASA-George C. Marshall Space Flight Center
Huntsville, AL 35812
Attn: C. E. Cataldo, S&E-ASTN-MX
Library

NASA-Goddard Space Flight Center
Greenbelt, MD 20771
Attn: Library

NASA-Langley Research Center
Hampton, VA 23365
Attn: J. H. Starnes
J. G. Davis, Jr.
M. C. Card
J. R. Davidson

NASA-Lewis Research Center
21000 Brookpark Road, Cleveland, OH 44135

Attn: Contracting Officer, MS 501-11
Tech. Report Control, MS 5-5
Tech. Utilization, MS 3-16
AFSC Liaison, MS 501-3
S&MTD Contract Files, MS 49-6
L. Berke, MS 49-6
N. T. Saunders, MS 49-1
R. F. Lark, MS 49-6
J. A. Ziemianski, MS 49-6
R. H. Johns, MS 49-6
C. C. Chamis, MS 49-6 (8 copies)
R. L. Thompson, MS 49-6
T. T. Serafini, MS 49-1
Library, MS 60-3 (2 copies)

NASA-Lyndon B. Johnson Space Center
Houston, TX 77001
Attn: S. Glorioso, SMD-ES52
Library

NASA Scientific and Tech. Information Facility
P.O. Box 8757
Balt/Wash International Airport, MD 21240
Attn: Acquisitions Branch (15 copies)

National Aeronautics & SpaceAdministration
Office of Advanced Research & Technology
Washington DC 20546
Attn: L. Harris, Code RTM-6
M. Greenfield, Code RTM-6
D. J. Weidman, Code RTM-6

National Aeronautics & Space Administration
Office of Technology Utilization
Washington DC 20546

National Bureau of Standards
Eng. Mech. Section
Washington DC 20234
Attn: R. Mitchell

National Science Foundation
Engineering Division
1800 G. Street, NW
Washington DC 20540
Attn: Library

Northrop Corporation Aircraft Group
3901 West Broadway
Hawthorne, CA 90250
Attn: R. M. Verette
G. C. Grimes

Pratt & Whitney Aircraft
East Hartford, CT 06108
Attn: J. M. Woodward

Raytheon Co., Missile System Division
Mechanical Systems Laboratory
Bedford, MA
Attn: P. R. Digiovanni

Rensselaer Polytechnic Institute
Troy, NY 12181
Attn: R. Loewy

Rockwell International
Los Angeles Division
International Airport
Los Angles, CA 90009
Attn: L. M. Lackman
D. Y. Konishi

Sikorsky Aircraft Division
United Aircraft Corporation
Stratford, CT 06602
Attn: Library

Southern Methodist University
Dallas, TX 75275
Attn: R. M. Jones

Space & Missile Systems Organization
Air Force Unit Post Office
Los Angeles, CA 90045
Attn: Technical Data Center

Structural Composites Industries, Inc.
6344 N. Irwindale Avenue
Azusa, CA 91702
Attn: R. Gordon

Texas A&M
Mechanics & Materials Research Center
College Station, TX 77843
Attn: R. A. Schapery
Y. Weitsman

TRW, Inc.
23555 Euclid Avenue
Cleveland, OH 44117
Attn: I. J. Toth

Union Carbide Corporation
P. O. Box 6116
Cleveland, OH 44101
Attn: J. C. Bowman

United Technologies Research Center
East Hartford, CT 06108
Attn: R. C. Novak
Dr. A. Dennis

University of Dayton Research Institute
Dayton, OH 45409
Attn: R. W. Kim

University of Delaware
Mechanical & Aerospace Engineering
Newark, DE 19711
Attn: B. R. Pipes

University of Illinois
Department of Theoretical & Applied Mechanics
Urbana, IL 61801
Attn: S. S. Wang

University of Oklahoma
School of Aerospace Mechanical & Nuclear Engineering
Norman, OK 73069
Attn: C. W. Bert

University of Wyoming
College of Engineering
University Station Box 3295
Laramie, WY 82071
Attn: D. F. Adams

U. S. Army Materials & Mechanics Research Center
Watertown Arsenal
Watertown, MA 02172
Attn: E. M. Lenoe
D. W. Oplinger

V.P. I. and S. U.
Dept. of Eng. Mech.
Blacksburg, VA 24061
Attn: R. H. Heller
H. J. Brinson
C. T. Herakovich
K. L. Reifsnider

End of Document